Article

Calcitriol promotes differentiation of glioma stem-like cells and increases their susceptibility to temozolomide

Julia Gerstmeier[1,#], Anna-Lena Possmayer[1,#], Süleyman Bozkurt[2], Marina E. Hoffmann[2], Ivan Dikic[2], Christel Herold-Mende[3], Michael Burger[4], Christian Münch[2], Donat Kögel [1,5] and Benedikt Linder[1,*]

[1] Experimental Neurosurgery, Dept. of Neurosurgery, Neuroscience Center, Goethe University Hospital, Goethe University; 60590 Frankfurt am Main, Germany (J.G.: Julia.gerstmeier@outlook.de; A.L.P: annalena.possmayer@gmail.com; B.L.: linder@med.uni-frankfurt.de; D.K.: koegel@em.uni-frankfurt.de)

[2] Institute of Biochemistry II, Faculty of Medicine, Goethe University Frankfurt, 60590 Frankfurt am Main, Germany (S.B.: Bozkurt@med.uni-frankfurt.de: (M.H.: Hoffmann@med.uni-frankfurt.de; C.M.: ch.muench@em.uni-frankfurt.de; I.D. ivan.dikic@biochem2.de)

[3] Division of Experimental Neurosurgery, Department of Neurosurgery, University Hospital Heidelberg, INF400, 69120 Heidelberg, Germany; (C.H.M.: Christel.Herold-Mende@med.uni-heidelberg.de)

[4] Dr. Senckenberg Institute of Neurooncology, Goethe University Hospital, 60528 Frankfurt, Germany. (MB: michael.burger@kgu.de)

[5] German Cancer Consortium DKTK Partner site Frankfurt/Main, 60590 Frankfurt am Main, Germany and German Cancer Research Center DKFZ, 69120 Heidelberg, Germany

[#] These authors contributed equally

[*] Correspondence: linder@med.uni-frankfurt.de; Tel.: +49 69 6301 6930

Simple Summary: Cancer cells with a stem-like phenotype that are thought to be highly tumorigenic are commonly described in glioblastoma, the most common primary adult brain cancer. This phenotype comprises high self-renewal capacity and resistance against chemotherapy and radiation therapy, thereby promoting tumor progression and disease relapse. Here, we show that calcitriol, the hormonally active form of the "sun hormone" vitamin D_3, effectively suppresses stemness properties in glioblastoma stem-like cells (GSCs), supporting the hypothesis that calcitriol sensitizes them to additional chemotherapy. Indeed, a physiological organotypic brain slice model was used to monitor tumor growth of GSCs and the effectiveness of combined treatment with temozolomide, the current standard-of-care, and calcitriol was proven. These findings indicate that further research on applying calcitriol, a well-known and safe drug, as a potential adjuvant therapy for glioblastoma is both justified and necessary.

Abstract: Glioblastoma (GBM) is the most common and most aggressive primary brain tumor with a very high rate of recurrence and a median survival of 15 months after diagnosis. Abundant evidence suggests that a certain sub-population of cancer cells harbors a stem-like phenotype and is likely responsible for disease recurrence, treatment resistance and potentially even for the infiltrative growth of GBM. GBM incidence has been negatively correlated with the serum levels of 25-hydroxy-vitamin D_3, while the low pH within tumors has been shown to promote the expression of the vitamin D_3-degrading enzyme 24-hydroxylase, encoded by the *CYP24A1* gene. Therefore, we hypothesized that calcitriol can specifically target stem-like glioblastoma cells and induce their differentiation. Here, we show using in vitro limiting dilution assays, quantitative real-time PCR and ex vivo adult organotypic brain slice transplantation cultures that therapeutic doses of calcitriol, the hormonally active form of vitamin D3, reduces stemness to varying extent in a panel of investigated GSC lines and effectively hinders tumor growth of responding GSCs ex vivo. We further show that calcitriol synergizes with Temozolomide ex vivo to completely eliminate some GSC tumors. These findings indicate that calcitriol carries potential as an adjuvant therapy for a subgroup of GBM patients and should be analyzed in more detail in follow-up studies.

Keywords: Calcitriol; Vitamin D3; Glioblastoma; Glioblastoma stem-like cells

1. Introduction

Gliomas are tumors of the central nervous system of which the highest grade, glioblastoma (GBM, WHO grade IV glioma), is the most common and the most aggressive form [1]. These tumors are particularly resistant towards conventional chemotherapy, currently consisting of Temozolomide (TMZ)-based radiochemotherapy with the recent addition of Tumor-Treating Fields (TTF) [2-5]. The sensitivity of patients towards a TMZ-based therapy is dependent on the presence or absence of the enzyme O^6-methylguanine (O^6-MeG)-DNA methyltransferase (MGMT) and many GBM have a methylated MGMT-promoter-region and therefore do not express this enzyme [6]. The MGMT enzyme can repair the DNA damages induced by TMZ. A surgical resection of GBM is often not entirely possible due to highly infiltrative and diffuse growth of these tumors, which routinely leaves some undetectable tumor cells that cause frequent recurrences. All of those factors cause the devastatingly low 5-year survival-rate of less than 5% and a median survival of 15 months after diagnosis [7]. One mechanism by which treatment resistance and tumor recurrence is facilitated is the presence of a sub-population of cancer cells with a stem-like phenotype (GSCs, glioma stem-like cells; reviewed in [8]), which may be induced by several cues such as hypoxia [9], perivascular niches [10] or treatment borders such as the resection margin [11]. Key characteristics of the cells are that they have a higher differentiation potential, express various marker proteins associated with stemness such as SOX2, SOX9, OLIG2 and are considered more tumorigenic upon transplantation into rodents compared to their differentiated counterparts (reviewed in [8]).

Vitamin D_3 (VitD$_3$) is a steroidal hormone that is synthesized in the skin upon UV-B irradiation, which can alternatively be obtained through dietary sources, such as fatty fish or certain mushrooms [12]. In order to get activated, VitD$_3$ has to pass through two hydroxylation steps. The first hydroxylation occurs mainly in the liver to form 25-hydroxy vitamin D_3 (25(OH)D$_3$). This step is mediated by a 25-hydroxylase CYP2R1. CYP2R1 is the main 25-hydroxylase and promotes VitD$_3$ conversion in the liver, other enzymes with 25-hydroxylase activity, such as CYP27A1, exist in various other organs and can allow for local conversion [13]. The second hydroxylation occurs in the kidney and is mediated by 1α-hydroxylase (encoded by the gene CYP27B1), to form the hormonally active form $1\alpha,25(OH)_2$ vitamin D_3 ($1\alpha,25(OH)_2D_3$), also known as calcitriol. Similarly, calcitriol-synthesis can occur in multiple extra-renal sites including the brain [13]. 25(OH)D$_3$ is the major circulating form of VitD$_3$ and is frequently employed as a surrogate marker for the VitD$_3$ status. The degradation of 25(OH)D$_3$ and calcitriol is catalyzed by the 24-hydroxylase (encoded by the gene CYP24A1), the amount of calcitriol is therefore limited by both calcitriol catabolism and decreased amounts of 25(OH)D3 available for calcitriol synthesis [14,15]. Calcitriol acts by binding to the vitamin D receptor (VDR) which regulates target gene expression upon translocation to the nucleus. VDR signaling inhibits the expression of genes for calcitriol synthesis (e.g. CYP27B1) and activates VDR expression as well as the expression of genes responsible for calcitriol metabolism such as CYP24A1 (reviewed in [15]). The activation of genomic VDR signaling also induces anti-tumorigenic effects, like inhibition of proliferation, stimulation of differentiation processes and apoptosis [16]. In fact, the anti-tumorigenic effects of VitD$_3$ are well established and low 25(OH)D$_3$ serum levels are associated with increased cancer risk and mortality, indicating a tumor-preventive function of VDR signaling [15]. Interestingly a recent report demonstrated that acidosis, i.e. the acidic environment around tumors, enhances the stem-like state and mitochondrial respiration of GSCs, which was mediated by reduction of VitD$_3$ via 24-hydroxylase-mediated degradation, which was induced by the low pH [17].

It was recently shown that serum level of 25(OH)D$_3$ and the risk of GBM have an inverse relationship [18], indicating that patients with low 25(OH)D$_3$ have a higher risk to develop GBM. Similarly, Zigmont et al. observed that low prediagnostic 25(OH)D$_3$ levels and are associated with increased risk of glioma in men [19]. In addition, VDR-expression was found to be associated with improved overall survival [20]. Accordingly, calcitriol

and/or VitD₃ have been proposed as potential therapeutics for brain cancers [21,22]. Pre-clinical studies using differentiated GBM cell lines employed VitD₃-loaded nanoparticles to induce cytotoxicity in rat glioma cells [23] and combined VitD₃ with Temozolomide, leading to synergistic cytotoxicity via enhancement of autophagy [24]. Mechanistically it was shown that calcitriol induces senescence in conventional, FCS-grown glioma cell lines [25]. Importantly, a synthetic derivative of calcitriol, alfacalcidol, has already been tested in a small patient cohort in France as an adjuvant therapy and it was reported that from 11 patients analyzed (10 GBMs, 1 Anaplastic Astrocytoma [AA]) 3 patients showed continuous improvement and finally complete regression of the tumor (2 GBM, 1 AA) and the median survival of all patients was 21 months, with the two GBM responders still alive after 4 years of follow-up [26].

Taken together, these findings lead us to hypothesize that GSCs might be particularly vulnerable for a calcitriol-based therapy. As such, calcitriol should be able to induce differentiation and render GSCs more susceptible to conventional chemotherapeutics including TMZ.

2. Results

2.1 Calcitriol reduces stemness in GSCs in vitro

To analyze the potential for a calcitriol-based therapy, we made use of three previously described cell models: NCH644 [27]), GS-5 [28] and the primary culture 17/02 [29]. Using these three cell lines we performed limiting dilution assays (LDA) as described previously [29,30] and analyzed them using the Web-App ELDA [31]. In principle, the cells were treated using 10, 25 or 50 nM calcitriol or solvent (Ethanol, EtOH) immediately after seeding. After 7 days each well was evaluated for the presence of at least 1 sphere larger than 8 cells per well. We observed that calcitriol (Figure 1A to C) significantly reduced the sphere-forming potential ("stem-cell frequency") of NCH644 (Figure 1A) very strongly and significantly with a change in the stem-cell frequency from 1 in 23.3 after solvent-treatment to 1:81.6 and 1:119.1 after treatment with 10 and 25 nM calcitriol, respectively. The highest concentration of 50 nM calctriol induced an almost 10-fold reduction of 1:219.9. The effects on GS-5 (Figure 1B) and 17/02 (Figure 1C) were less pronounced. As such, the stem-cell frequency of GS-5 decreased from 1:188 (EtOH) to 1:206 (10 nM), 1:264 (25 nM) and 1:318 (50 nM), respectively. Only the ~2-fold reduction after treatment with 50 nM calcitriol reached statistical significance. Lastly, the stem-cell frequency of the primary line 17/02 changed from 1:153 after solvent-treatment to 1:152 (10 nM), 1:159 (25 nM) to 1:198 (50 nM) and neither was statistically different.

Next, we wondered if a clinically more applicable drug that is less calcemic than calcitriol, calcipotriol [32], exerts similar effects. Therefore, we also performed LDAs and found for all three cell lines (Figure 1D to F) similar, albeit less intense effects after treatment with 100 nM, 500 nM, 1000 nM calcipotriol or solvent. Specifically, calcipotriol led to a dose-dependent decrease of the stem-cell frequency of NCH644 cells (Fig .1D) from 1:50.6 (DMSO) to 1:80.5 (100 nM), 1:104 (500 nM) to 1:129.5 (1000 nM). Only the treatment with 500 nM and 1000 nM led to a statistically significant decrease. For GS-5 (Fig. 1E) and the primary line 17/02 (Fig. 1F) only the highest concentrations led to a statistically significant decrease in stem-cell frequency. Accordingly, the stem-cell frequency of GS-5 cells decreased from 1:190 (DMSO) to 1:241 (100 nM) to 1:232 (500 nM) and 1:310 (1000 nM), while it changed from 1:158 (DMSO) to 1:192 (100 nM) and 1:209 (500 nM) to 1:232 (1000 nM) in 17/02. The ratios and the respective p-values are summarized in table 1. From these experiments, we drew the conclusion that the synthetic derivative of calcitriol, calcipotriol is less potent than calcitriol. In order to describe the therapeutic effects evoked by VitD₃-signaling, we decided to perform all subsequent experiments only with calcitriol.
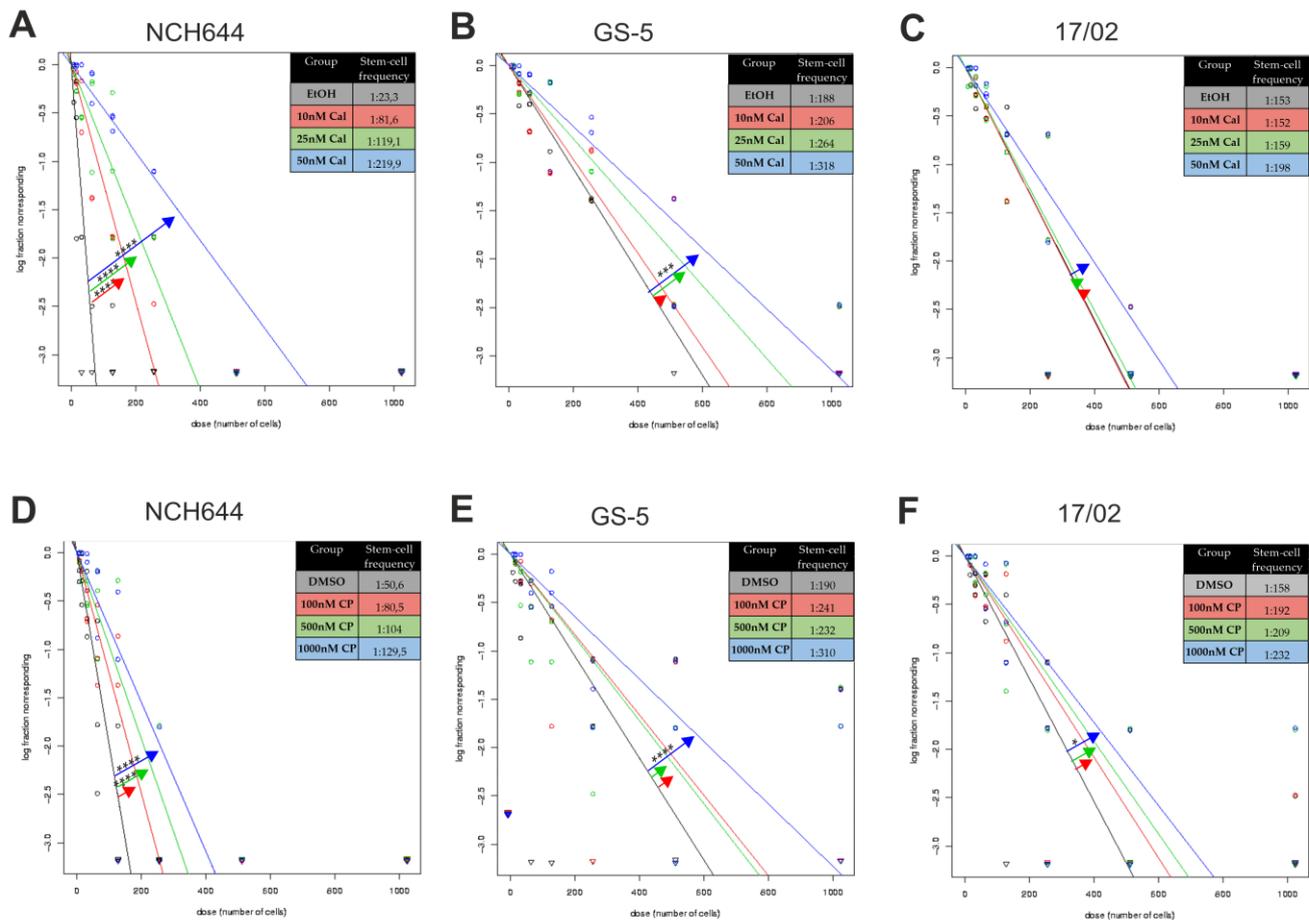
Figure 1. Calcitriol exerts differential activity among GSCs. (A to F) A log-fraction plot of the limited dilution model of data from (A and D) NCH644, (B and E) GS-5 and (C and F) 17/02 GSCs. The cells were treated with solvent (ethanol, EtOH; black) or (A to C) 10 (red), 25 (green) or 50 nM calcitriol (blue) or (D to F) 100 (red), 500 (green) or 1000 nM calcipotriol for 7 days after seeding the cell in dilution series from 1024 to 8 cells and analyzed the data using ELDA software [31]. The estimated stem-cell frequency is presented under each plot. The data are the summary of at least three experiment performed with 12 replicates per cell number and 8 different cell numbers seeded. *: p<0.05; **: p<0.01; ***: p<0.001; ****: p<0.0001; Chi-Square-Test from ELDA Web-App [31].

Table 1. Calculated stem-cell frequencies as determined using ELDA [31] of the GSCs NCH644, GS-5 and 17/02 7 days after treatment with calcitriol, calcipotriol or solvent (EtOH, DMSO, respectively) as indicated

Cell line	Calcitriol [nM]	Stem-cell frequency [1/X]	p-value (Chi²)	Calcipotriol [nM]	Stem-cell frequency [1/X]	p-value (Chi²)
NCH644	EtOH	23.3		DMSO	50.6	
	10	81.6	1.46e-15	100	80.5	0.00314
	25	119.1	3.01e-25	500	104	5.05e-06
	50	219.9	1.12e-43	1000	129.5	4.58e-09
GS-5	EtOH	188		DMSO	190	
	10	206	0.525	100	241	0.0861
	25	264	0.0245	500	232	0.140
	50	318	0.00061	1000	310	0.000556
17/02	EtOH	153		DMSO	159	

10	152	0.97	100	192	0.191
25	159	0.81	500	209	0.0627
50	198	0.101	1000	232	0.0109

During microscopic evaluation of the LDAs we observed -especially for the well-responding GSC line NCH644- not only fewer spheres can form, but that those that could form were markedly smaller. This is exemplified in Figure 2 showing that compared to solvent treatment (Fig. 2A), 10 nM calcitriol (Fig. 2B) and 50 nM calcitriol (Fig. 2C) dose-dependently reduce the amount and size of spheres. This indicates that the analyses using ELDA rather understates the true effect size of calcitriol-treatment.
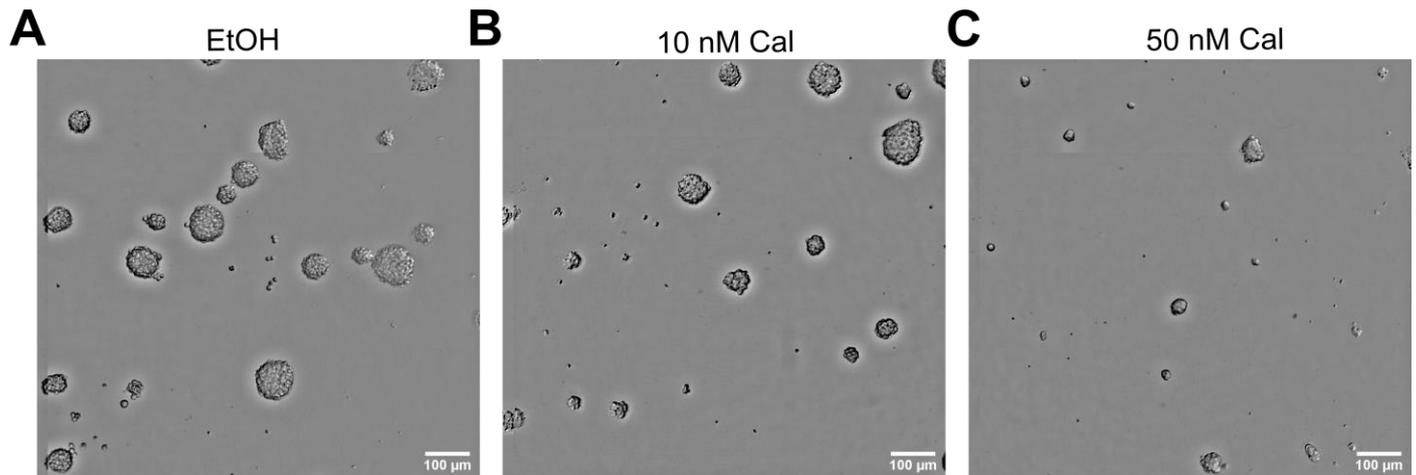

Figure 2. Calcitriol reduces NCH644 sphere size and number. Photomicrographs of NCH644 GSCs 7 days after treatment with (A) solvent (ethanol, EtOH), (B) 10 nM calcitriol (Cal) or (C) 50 nM Cal. Pictures were taken with a Tecan Spark plate-reader and images were cropped using FIJI [33].

These findings prompted us to analyze the response of the GSCs in more detail and we therefore developed a semi-automatic FIJI-macro to analyze sphere area and number (Fig. 3). For NCH644 this approach showed that increasing doses of calcitriol from 10 to 25 and 50 nM significantly reduces the mean sphere number per well (Fig. 3A) as well as the median sphere area (Fig. 3B). Specifically, the average sphere number and median area of solvent treated cells was 41 and 656 μm^2, respectively. Treatment with 10 nM, 25nM or 50 nM reduced these numbers to 24 spheres with a median size of 510 μm^2, 27 spheres with a median size of 506 μm^2 and 15 spheres with 427 μm^2, respectively. For GS-5 only the highest dose of 50 nM calcitriol significantly reduced the number of spheres per well (Fig. 3C) compared to solvent treated cells. As such the mean number of spheres per well was reduced from 71 after solvent-treatment to 58, 71 and 51 after treatment with 10 nM, 25 nM and 50 nM, respectively. The median sphere size (Fig. 3D) was 343 μm^2 after solvent-treatment and remained at 329 μm^2 after treatment with 50 nM calcitriol. Lastly, the primary culture 17/02 showed neither a reduction in sphere number (Fig. 3E) nor sphere area (Fig. 3F), with an average sphere number and median size of 33 spheres and 420 μm^2 after solvent-treatment and 32 spheres and 414 μm^2 after 50 nM calcitriol, respectively.
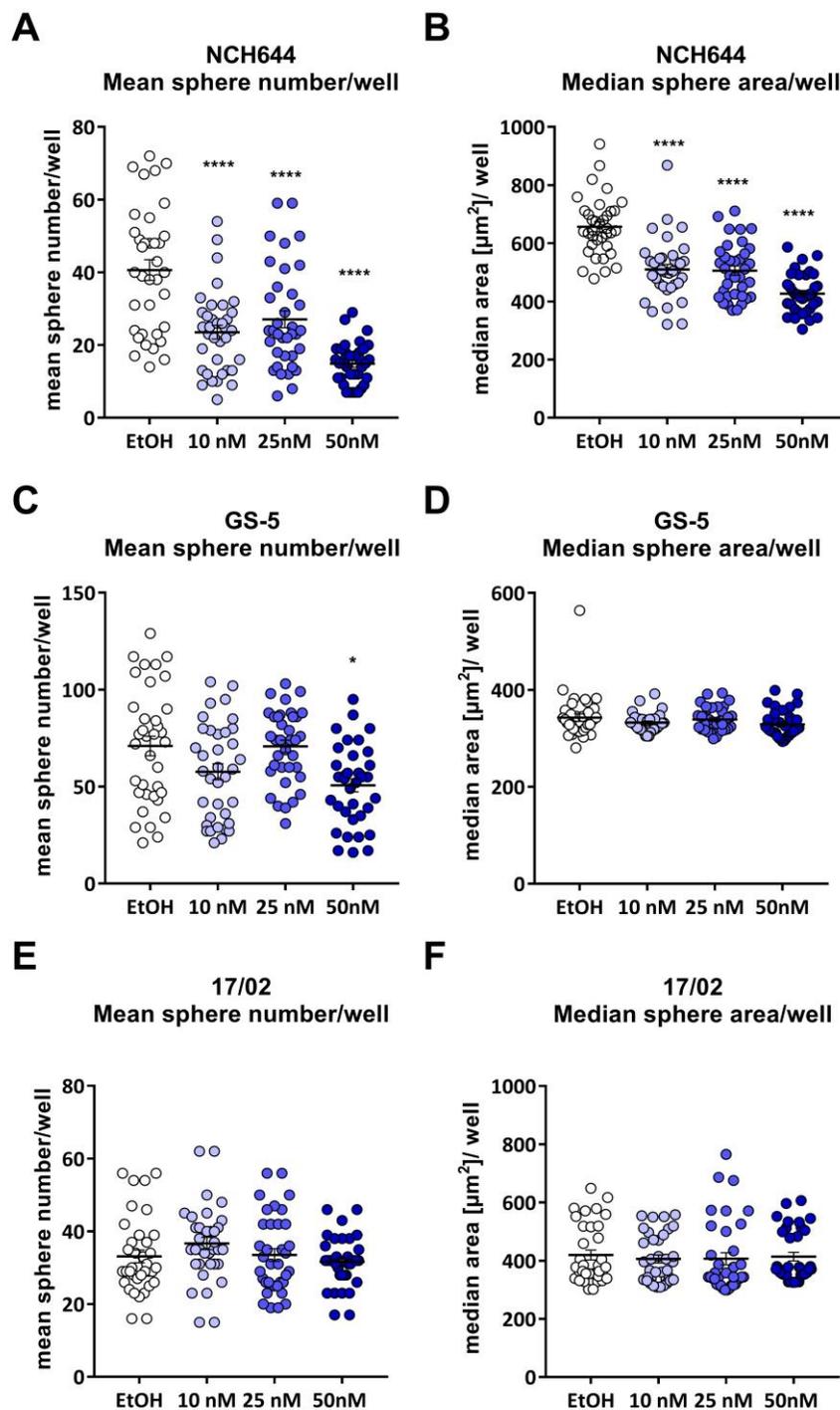
Figure 3. Calcitriol reduces sphere number and sizes of NCH644 and to a lesser extent in GS-5 GSCs. (A and B) Point-Plots of NCH644 GSCs 7 days after treatment with solvent (ethanol, EtOH), 10 nM calcitriol (Cal, light blue), 25 nM Cal (blue) or 50 nM Cal (dark blue) after seeding of 512 cells after analyses using a self-made FIJI-macro to measure (A) sphere number, (B) median sphere size. (C and D) Point-Plots of GS-5 GSCs 7 days after seeding of 1024 and treatment as in (A). (E and F) Point-Plots of 17/02 primary GSCs 7 days after seeding of 512 cells as in (A). *: p<0.05; **: p<0.01; ***: p<0.001; ****:p<0.0001; One-Way ANOVA Dunnett's multiple comparisons test.

2.2 Differential activity of calcitriol

The fact that we observed such pronounced differences between the three GSC lines argued for cell line-/tumor-specific therapeutic effects of calcitriol and prompted us to further expand our cell panel. We therefore analyzed additional 7 GSC lines including 4

locally established primary lines. The additional 4 primary lines are MNOF1244, which has not been described previously (see materials and methods), 17/01 [29], MNOF1300 [34] and the primary gliosarcoma line MNOF168 [35]. In addition, we also included 3 cell lines established and described in the literature GS-73 [36], NCH421k [27] and NCH481 [37]. We analyzed the sensitivity of the cells using LDAs after treatment with 50 nM calcitriol for 7 days and calculated the fold-change in stem-cell frequency to better compare the results from the different cell lines. This analysis (Fig. 4A) revealed that 6 out of 10 lines (60 %) show a significant reduction in stem-cell frequency after calcitriol-treatment (vertical cut-off line in Fig. 4 A). Importantly, two lines (NCH644 and NCH421k) show an exceptionally strong response to calcitriol with a more than 9- and 7-fold reduction in stem-cell frequency. Next, we hypothesized that differences in calcitriol-sensitivity might be, at least partially, due to differences in VDR expression and analyzed VDR mRNA expression via qRT-PCR and plotted it against the calcitriol-response (Fig. 4 B). This approach revealed on the one side that profound differences of VDR expression occur between the cell lines ranging over almost three magnitudes from 0.00177 (GS-73) to 1.63088 (NCH644). On the other side, we determined that a very strong correlation (Pearson R: 0.9828, p value < 0.0001) exists between calcitriol-sensitivity and receptor expression.
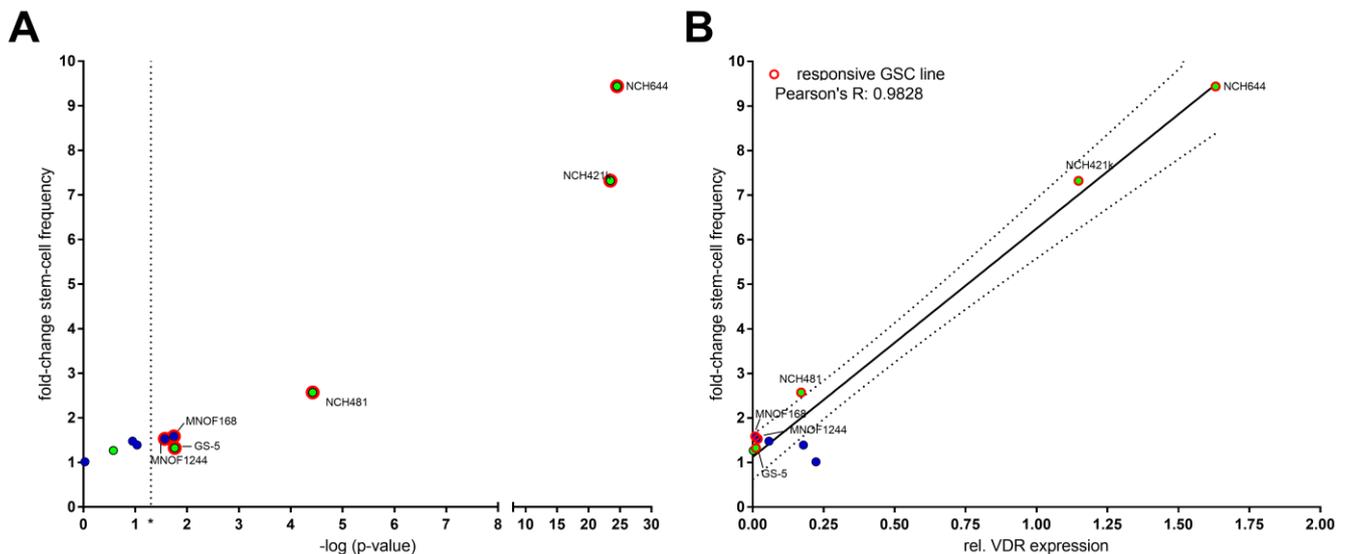

Figure 4. Differential sensitivity to calcitriol strongly correlates with VDR expression. (A) Point-Plot of the relative fold-change in stem-cell frequency after performing a limiting dilution assay after treatment with 50 nM calcitriol or solvent for 7 days after seeding of 1024 to 8 cell per well. The stem-cell frequency was determined using ELDA [31] and the change in stem-cell frequency was calculated and plotted against the –log p-value (Chi²) of the ELDA-analysis. (B) Point-Plot of the relative fold-change in stem-cell frequency as in (A) plotted against the relative VDR-expression and Pearson correlation (black line + 95 confidence interval; dotted line). Locally established primary cultures are depicted with blue dots, non-primary cultures with green dots. GSCs with a significant reduction in stem-cell frequency (dotted line in A) are labeled and marked by red outlines in both sub-figures.

2.3 Calcitriol reduces stemness-associated marker genes

Hereafter we were interested in the gene expression changes that are induced by calcitriol-treatment. Therefore, we treated the cells for 24 and 48 h with 10 and 50 nM calcitriol and analyzed target gene expression (Figure 5). Using this approach we can show that, expectedly, *CYP24A1* expression (Figure 5A) is strongly induced after both 24 and 48h. Additionally, we analyzed *GLI1* (Figure 5B) as a marker for Hedgehog pathway activity, because this pathway is described to be important for GSC stemness [38] and there is evidence including our previous studies [39,40] that calcitriol is a direct inhibitor of this pathway. Nonetheless, only a small, non-significant, tendency towards inhibition can be

observed after calcitriol-treatment. The analyses of the three stemness marker genes (Figure 5C to E) *OLIG2, SOX2* and *SOX9* showed that after 24h *OLIG2* (Figure 5C) expression is significantly reduced after 50 nM calcitriol treatment and after 48h after both 10 and 50 nM treatment. *SOX2* (Figure 5D) is significantly reduced 24h after treatment with 10 and 50 nM calcitriol, whereas after 48h of treatment only the 50 nM treatment still elicits a significant reduction. *SOX9* (Figure 5E) only shows a slight tendency towards inhibition after 24h of treatment, but no change after 48h. Analyses of the differentiation marker GFAP (Figure 5F) showed a pronounced increase after 24h, yet only the 10 nM treatment was statistically significant. 48h after treatment *GFAP*-expression was further increased and statistically significant after treatment with 50 nM calcitriol. Lastly, we measured *BCL2*-expression (Figure 5G) and *CCND1* (encoding for Cyclin D1) (Figure 5H) which are known to be negatively regulated by active VDR signaling [15], but no significant changes were observed, although a slight tendency is apparent for *BCL2*-expression 48h after treatment with 50 nM calcitriol.
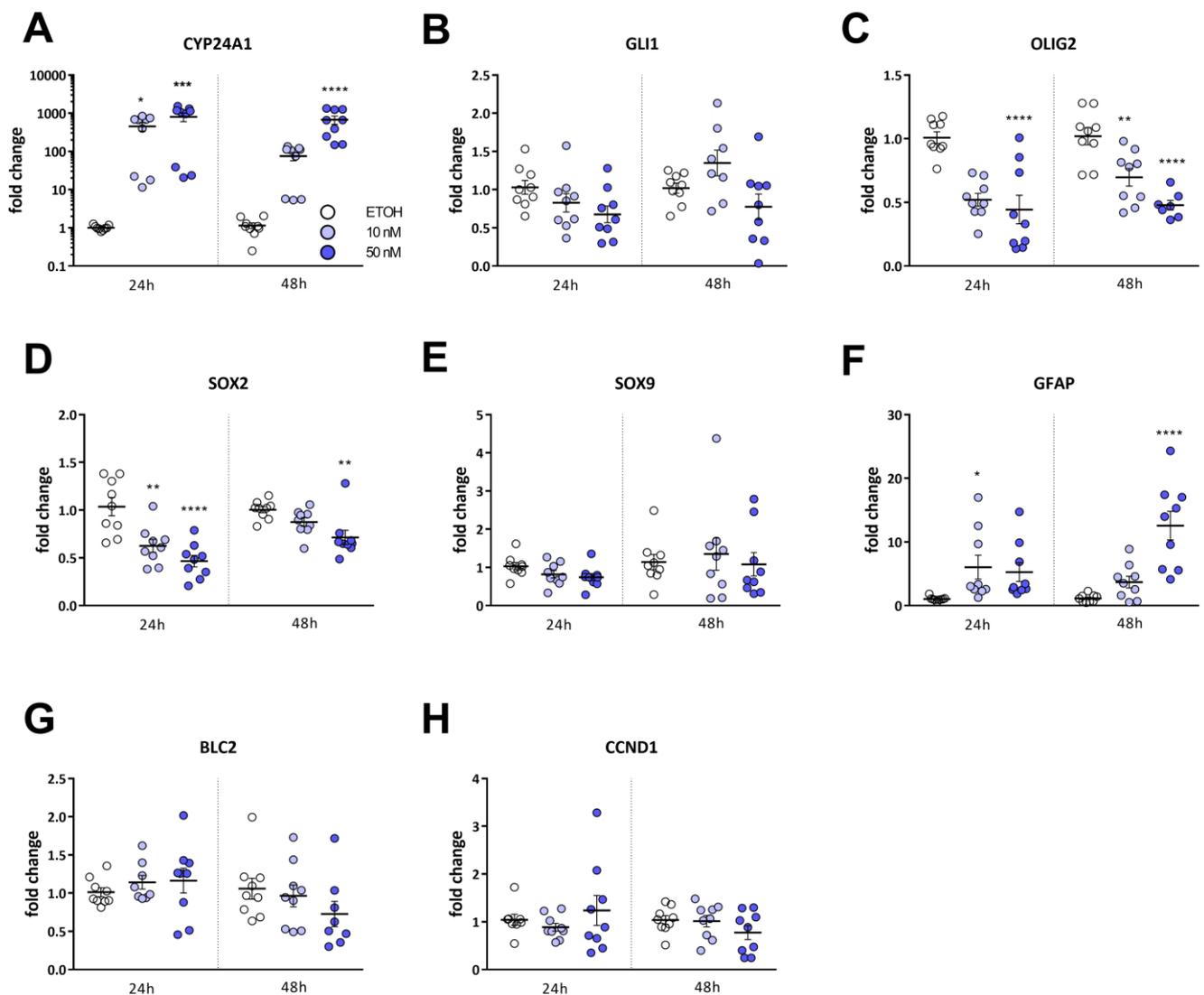

Figure 5. Calcitriol-induced changes in gene expression are indicative of reduced stemness. Point-plots of Taqman-based gene expression of NCH644 GSCs after treatment with solvent (ethanol, EtOH), 10 (light blue) or 50 (dark blue) nM calcitriol (Cal) for 24 or 48h. The data are the summary of three experiments performed in triplicates. *: p<0.05; **: p<0.01; ***: p<0.001; ****: p<0.0001; One-Way ANOVA with Dunnett's multiple comparisons test.

Using immunofluorescent stainings (Figure 6) we confirmed the reduction of SOX2 (Figure 6A and D), OLIG2 (Figure 6B and E) and the increase in GFAP-expression (Figure 6C and F) 72h after treatment with 50 nM calcitriol. A quantification (Figure 6D to F) using FIJI showed that the relative signal intensity of SOX2 and OLIG2 decreased to 52% and 53%, respectively, relative to solvent treated cells (100%). In contrast, GFAP-expression increased to 226% compared to solvent, while it should be noted that several cells exhibit a very pronounced increase of more than 300%.
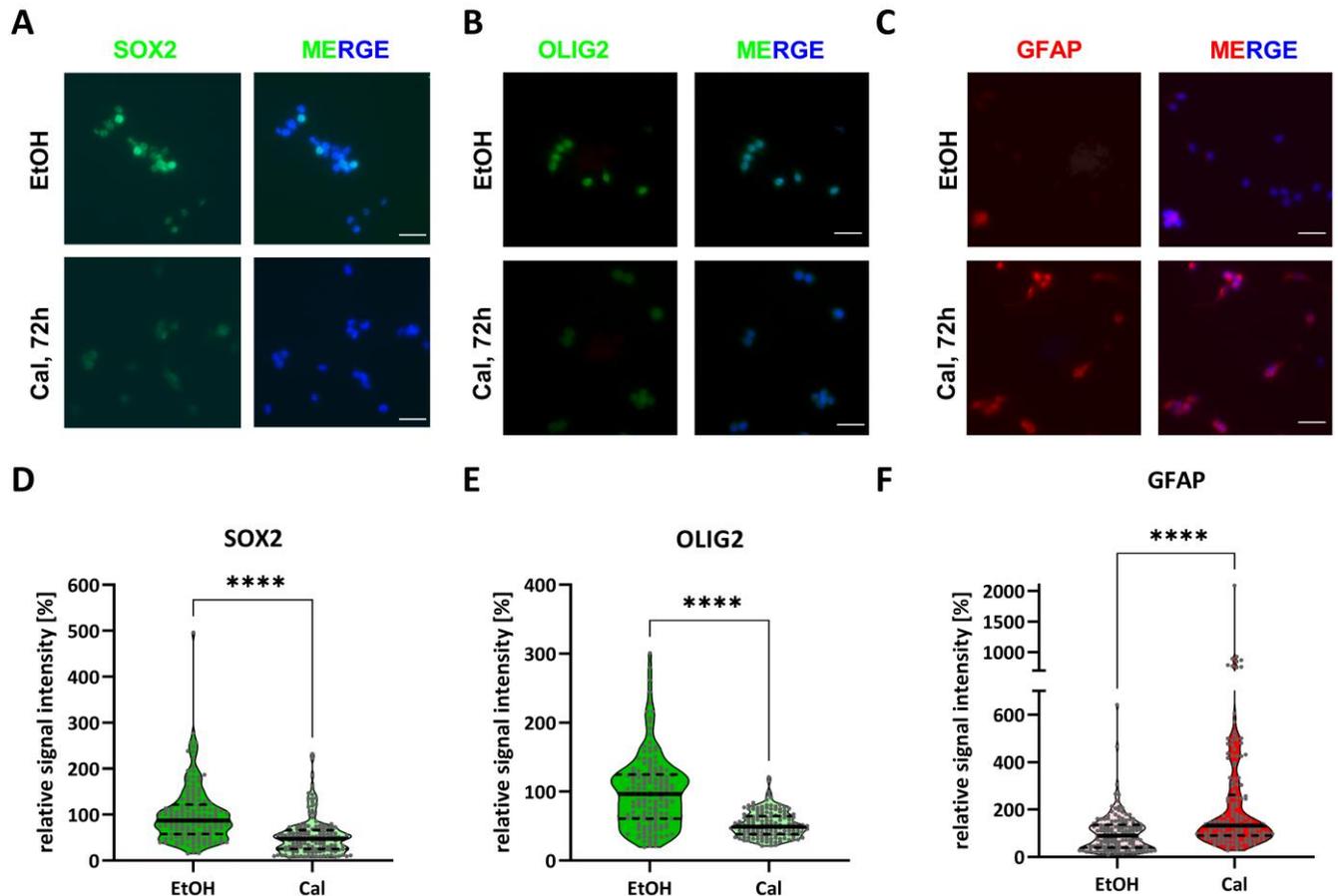

Figure 6. Calcitriol reduces SOX2 and OLIG2 stemness marker expression and increases GFAP differentiation marker expression. (A to C) Representative immunofluorescence pictures of NCH644 GSCs 72h after treatment with 50 nM calcitriol (Cal) or solvent (EtOH) and (D and F) Violin plots of the quantification of 50 cells from at least three random vision fields of three independent experiments after staining against (A and D) SOX2, (B and E) OLIG2 and (C and F) GFAP. The solid horizontal line marks the median and the dashed lines separate the quartiles. *: $p<0.05$; **: $p<0.01$; ***: $p<0.001$; ****: $p<0.0001$; two-tailed t-test.

2.4 Alterations in global proteomic profiles after calcitriol treatment

To characterize the effects on global protein levels and to gain a more detailed understanding of the calcitriol-effects, we performed quantitative LC-MS/MS. Hierarchal Euclidean clustering analysis showed that replicates of 50nM calcitriol treatment (48h) distinctly differs from solvent and therefore they were clustered together (Figure 7A). Then to determine which proteins were affected the most, we calculated fold differences and significances by two-sided, unpaired Student`s t-test of each protein. Stemness markers like OLIG2 and SOX2 were significantly reduced which supports our finding in qPCR and immunofluorescence analysis of these two markers in protein level. It was also determined that most of Ca^{2+}-related and $VitD_3$-target proteins were significantly upregulated

upon calcitriol treatment for 48 hours (Figure 7B). Then we indicated the findings of these proteins with cluster analysis on heatmaps. With the sole exception of AHNAK2, all the altered Ca^{2+}-related proteins found, i.e. CAPN5, ANXA2, ANXA5, RCAN1, and S100A6 were increased, suggesting that calcitriol might activate Ca^{2+}-related pathways (Figure 7C). CYP24A1 protein levels were significantly elevated (nearly 25-fold) which was strongly correlated with CYP24A1 mRNA levels as well as other $VitD_3$-target proteins: G6PD, LPGAT1, CLMN, ASAP2 and S100A6 were also increased along with CYP24A1 (Figure 7D). Furthermore, our proteomic analysis showed an elevation of actin/microtubule related proteins; CCT6B, PALLD, ARPC1B, MREG, PACSIN3, AFAP1L2, and TACC2 upon 48-hour calcitriol treatment.
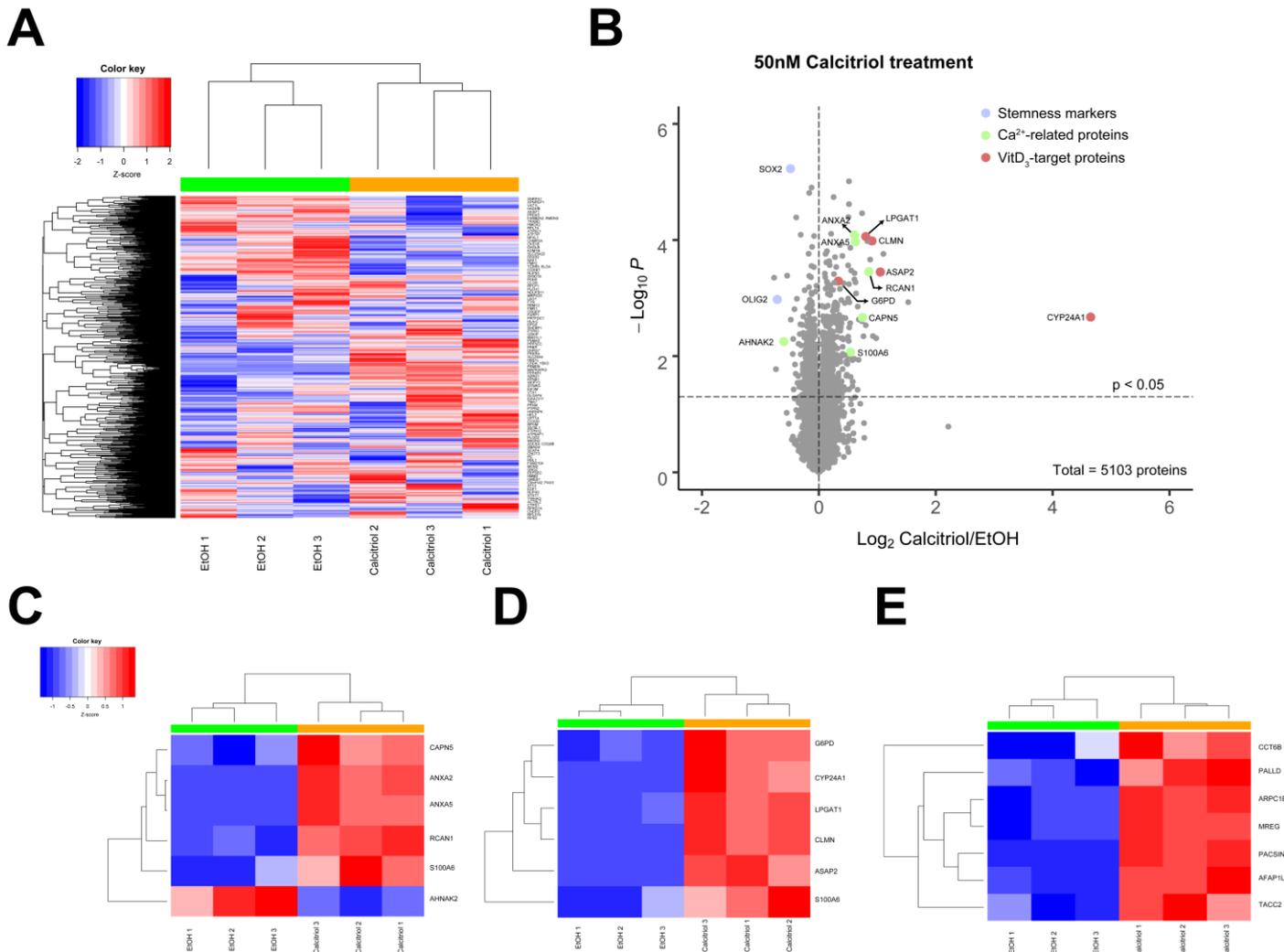

Figure 7. The effect of 48 hours of calcitriol treatment on global protein levels. (A) Hierarchal Euclidean clustered whole proteome indicates calcitriol similarly grouped and distinct profile of proteins. (B) Volcano plot showing fold changes of calcitriol versus solvent for all quantified proteins. The stemness markers, Ca2+-related and vitamin D3-target proteins are also indicated color coded on the plot. Heatmap representation of Ca2+-related (C), vitamin D3-target (D) and actin/microtubules-related proteins (E)

2.4 Calcitriol reduces tumor growth ex vivo and synergizes with TMZ

Based on the data obtained so far, we hypothesized that calcitriol has the potential as a "differentiation therapy". This in turn would imply that calcitriol-treated cells are more sensitive towards conventional chemotherapy such as TMZ. To test this hypothesis, we first generated GFP-expressing NCH644 (NCH644 GFP⁺) and NCH421k (NCH421k GFP⁺) cells and applied them in an *ex vivo* tumor growth assay using organotypic tissue culture

(OTC) as described recently [29,41]. For this purpose, the OTCs were prepared and one day after tumor transplantation (termed d0) they were treated 3 times per week using solvent (DMSO for TMZ; EtOH for calcitriol), TMZ, calcitriol or a combination of both. For NCH644 (Fig. 8), images were taken at day 3, 5, 7 and 10 to measure tumor sizes with representative images being depicted in figure 8A. To better compare the dynamics of tumor growth/regression, we normalized the sizes of each tumor to its size at d0. This approach showed that over time (Figure 8B) solvent-treated tumors (black points/lines) grew continuously. TMZ alone only mildly and non-significantly reduced the tumor areas, which is in line with the concept that GSCs are largely resistant to conventional therapy. In contrast, calcitriol single treatment effectively halted tumor growth of most tumors. Furthermore, other tumors even show complete remission after calcitriol single agent treatment (8 of 24, 33,33%%). Both cases are exemplified in Fig. 8A. Finally, the combination treatment synergistically and statistically significantly reduces tumor sizes and leads to the disappearance of several tumors as well (7 of 27, 25,93%). Specifically, solvent-treated tumors grew to 3.7, 6.0 and 9.8-fold of their initial size after 5 (Fig. 8C), 7 (Fig. 8D) and 10 days (Fig. 8E), while TMZ alone slowed the growth non-significantly to the 2.8, 3.0 and 5.9-fold. Calcitriol-treated tumors were on average 1.1, 1.4 and 2.2-fold of their initial size and the difference was statistically significant for each time point. Importantly, the combination treatment resulted, on average, to 0.8, 0.9 and 1-fold tumor growth compared to the initial size. This difference was highly significant against solvent and TMZ for all timepoint and also against calcitriol-single-treatment after 10 days of treatment, suggesting a potential synergism.
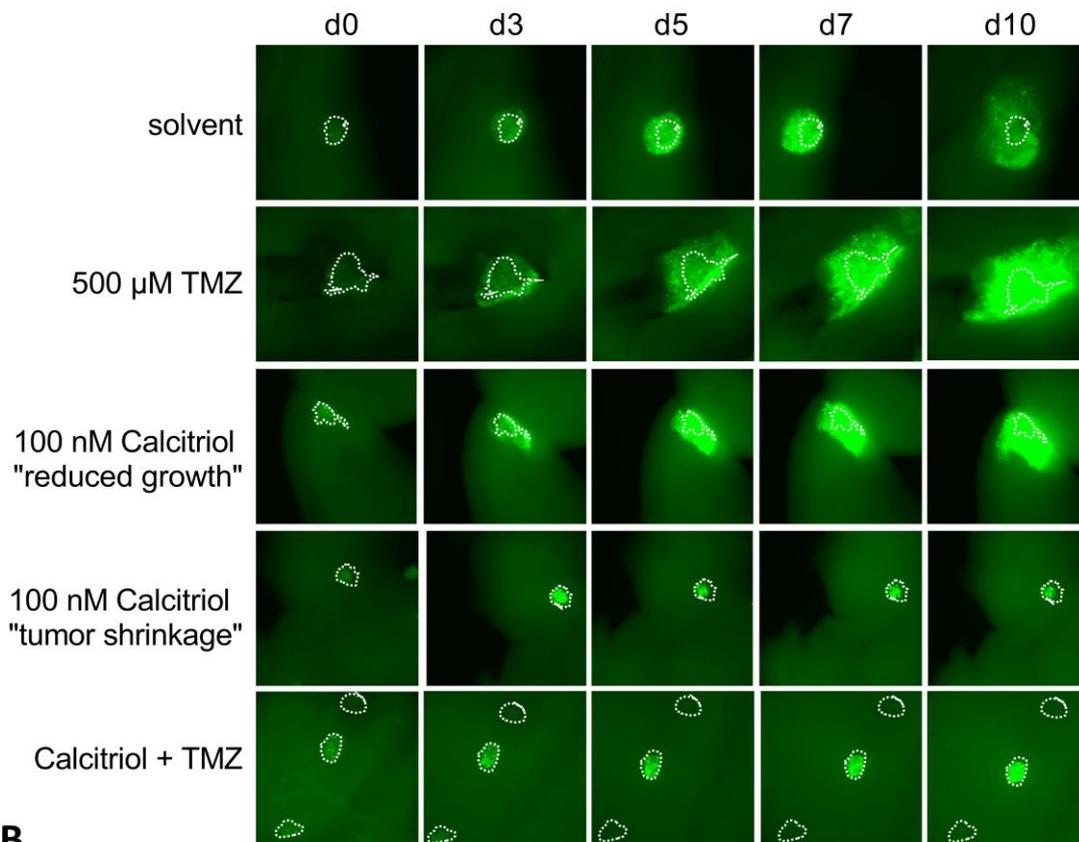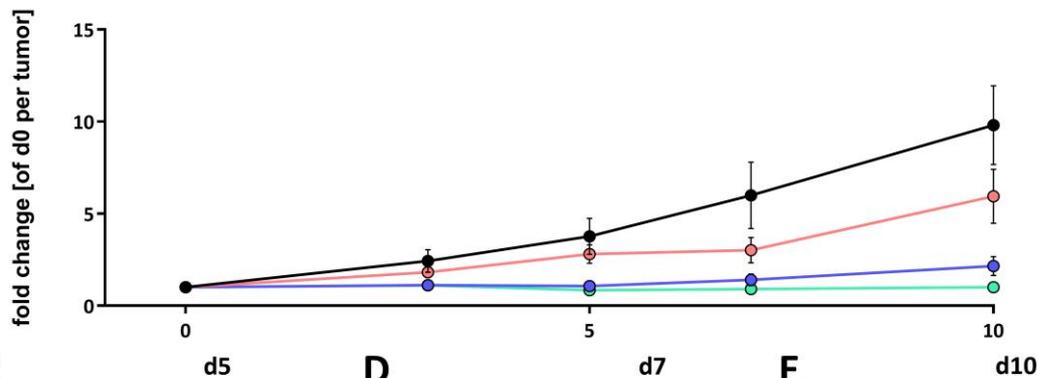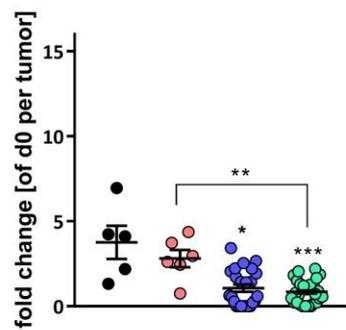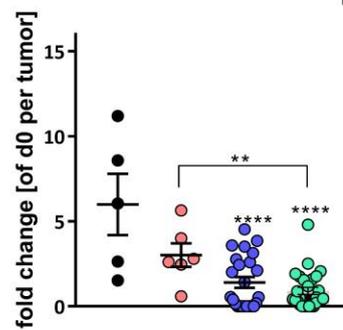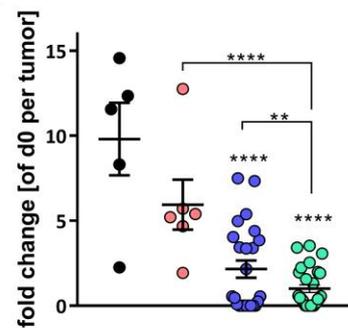
Figure 8. Calcitriol halts tumor growth and synergizes with TMZ in an ex vivo organotypic tissue culture tumor growth kinetics. A) Representative Microphotographs of NCH644 GFP+ tumors transplanted onto adult murine brain organotypic tissue culture slices after treatment with solvent (DMSO for TMZ; EtOH for calcitriol), 500 μM TMZ, 100 nM calcitriol (Cal) or a combination of both for the times as indicated. B) Growth curves of the NCH644 GFP+ tumors normalized to the

size of tumor d0 after treatment as in A) depicted as the mean +/- SEM. C to E) Point-plot of the data summarized in B) after treatment for C) 5 days, D), 7 days and E) 9 days as in A). *: $p<0.05$; **: $p<0.01$; ***: $p<0.001$; ****:$p<0.0001$; Two-Way ANOVA with Tukey's multiple comparisons test.

Similar results have been observed for NCH421k GFP+ (Fig. 9), although these tumors appear to be more sensitive towards TMZ. As such solvent-treated tumors continuously grow and reach the 2.9-, 9.1- and 17.1-fold of their initial size on average at d5 (Fig. 9C), d12 (Fig. 9D) and d16 (Fig. 9E), respectively. Treatment with TMZ reduced the growth of the tumors continuously leading to an average tumor size that is 2.1- (d5), 0.9-(d12) and finally 0.4-fold (d16) compared to the initial tumor. The difference between solvent- and TMZ-treated tumors reached statistical significance after 12 and 16 days. Calcitriol-treatment already blocked tumor growth to 0.6-fold after 5 days. This could be further decreased to 0.3- (d12) and finally 0.1-fold (d16) of the initial tumor, while achieving statistical significance at d12 and d16. The combination of both was also highly effective, but did not differ significantly from either treatment. The average tumor size after combination treatment was 1.1- (d5), 0.4- (d12) and 0.3-fold (d16) compared to the initial size. Thus, no synergism can be inferred for NCH421k tumors.
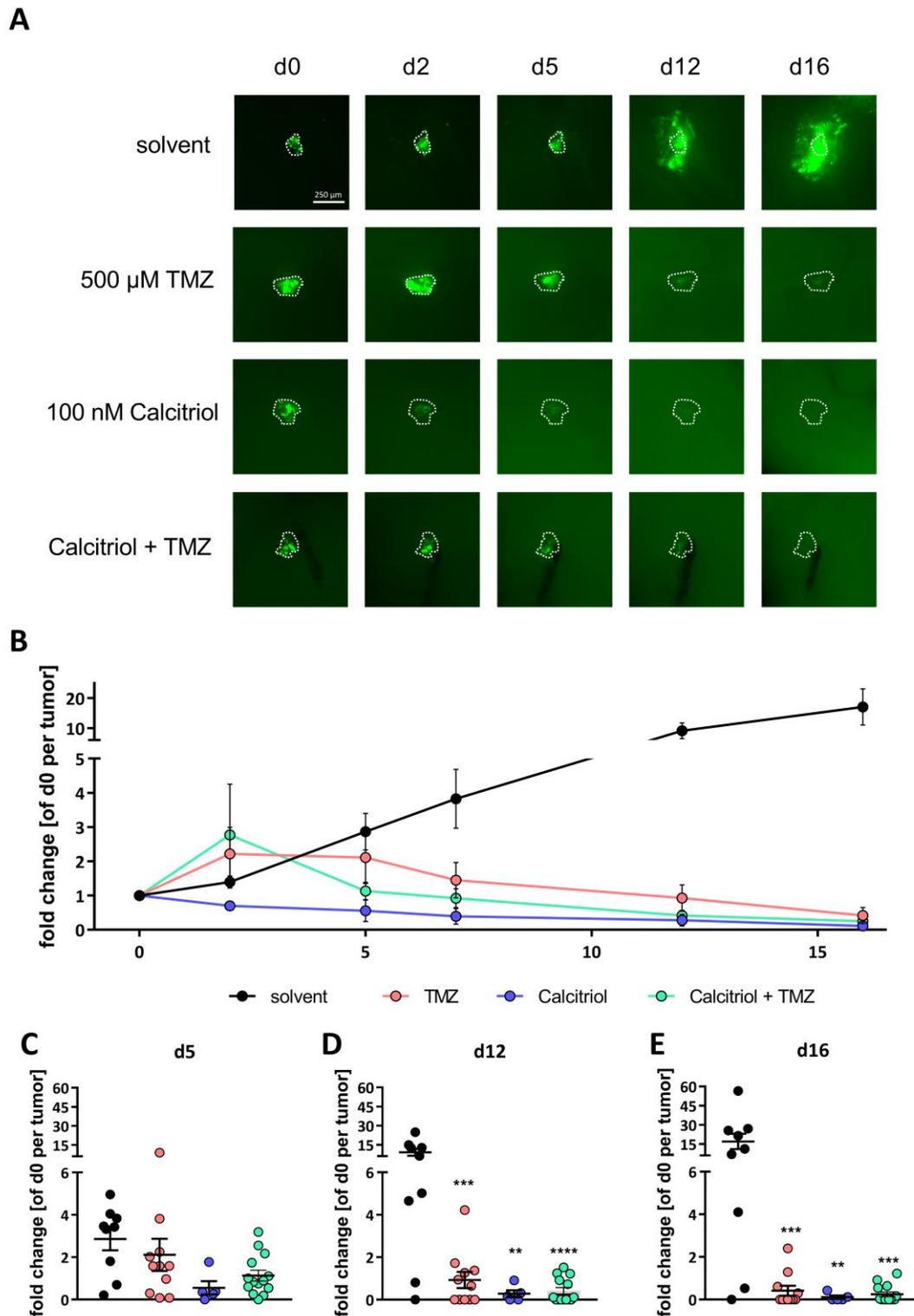
Figure 9. Calcitriol and TMZ prevent tumor growth in an ex vivo organotypic tissue culture tumor growth kinetics. A) Representative Microphotographs of NCH421k GFP⁺ tumors transplanted onto adult murine brain organotypic tissue culture slices after treatment with solvent (DMSO for TMZ; EtOH for calcitriol), 500 μM TMZ, 100 nM calcitriol (Cal) or a combination of both for the times as indicated. B) Growth curves of the NCH421k GFP⁺ tumors normalized to the size of tumor d0 after treatment as in A) depicted as the mean +/- SEM. C to E) Point-plot of the data summarized in B) after treatment for C) 5 days, D), 12 days and E) 16 days as in A). *: $p<0.05$; **: $p<0.01$; ***: $p<0.001$; ****: $p<0.0001$; Two-Way ANOVA with Tukey's multiple comparisons test.

3. Discussion

Cancer recurrence generally leads to more aggressive and treatment resistant disease, which finally culminates in the death of patients. Due to the highly infiltrative tumor growth, it is impossible to achieve microscopic complete resection in patients with GBM and it is proposed that the remaining cells can obtain and harbor a stem-like phenotype which is crucial to replenish the tumor [42,43]. It has been further hypothesized that these GSCs reside in either hypoxic niches [9], perivascular niches [10] or at treatment borders, such as the resection margin [11]. Accordingly, many attempts are being made at specifically targeting this phenotype [44-48]. The anti-cancer and differentiation-promoting activity of VitD$_3$ and calcitriol have been known for some time and it has been shown in numerous studies that intake of VitD$_3$, a safe and well-studied drug, can prevent cancer occurrence [15,22,49].

Based on these two paradigms, i.e. its known ability to target the cancer stem-like phenotype and its anti-tumorigenic activity, we decided to apply therapeutic doses of calcitriol, the hormonally active form of VitD$_3$, in an aim to reduce the stem-like phenotype of GSCs and thereby increase their sensitivity to chemotherapy. Accordingly, our studies revealed - to our knowledge for the first time - that treatment with 10, 25, and 50 nM Calcitriol decreases stemness in three GSC lines. Notably, the treatment efficiency varied between the cell lines. Some GSCs, for example NCH644, seem to be more sensitive to calcitriol treatment than GS-5, which showed a moderate response and 17/02, which barely showed any response at all. Importantly, these findings are in line with previous results obtained in the clinical setting by Trouillas et. al. [26]. The authors of this study gave the synthetic VitD$_3$-derivative alfacalcidol as an adjuvant therapy to 11 patients (10 GBM, 1 Anaplastic Astrocytoma (AA, grade III glioma)). Of those 11 patients three (2/11 GBMs, 1/1 AA) experienced continuous improvement and finally complete tumor regression. Accordingly, the median survival of this study cohort was 21 months, which is considerably higher than the reported ~13 months found in the recent literature. The two GBM responders were still alive after 4 years of follow-up [26]. One possible hypothesis derived from these preliminary observations is that a certain sub-population (~20%) of patients may show increased sensitivity towards a VitD$_3$-based therapy. This hypothesis is consistent with our analyses of an extended cell panel of 10 GSC cultures. Of those, 60% show a significant response, whereas 20% (NCH644 and NCH421k) very strongly responded to calcitriol both in vitro and ex vivo, providing a solid starting point to experimentally determine molecular factors mediating calcitriol sensitivity in GBM.

Another pertinent question concerns the most effective drug for a VitD$_3$-based therapy. Here we compared the effect obtained by calcitriol to that of its synthetic, less-calcemic [32], derivative calcipotriol. We observed similar effects of both compounds, although the intensity was comparatively weaker after treatment with calcipotriol, which prompted us to focus our studies on the effects of calcitriol. Another group reported the usage of calcipotriol in T98G serum-grown GBM cells [50]. Similar to our approach the authors compared calcipotriol to calcitriol and another derivative, tacalcitol, and found that calcitriol is the most effective drug, although they applied very high doses of calcitriol (up to 10 μM). Although several studies can be found which employ various VitD$_3$-derivatives, for example calcipotriol in pancreatic cancer cells [51,52], comparative approaches are scarce. Using breast cancer cell lines a comparison between calcitriol, calcipotriol and EB1089, another VitD$_3$-derivative, was conducted by performing combination treatment with the chemotherapeutic gefitinib [53]. The authors observed synergy of all compounds with the chemotherapy, but no discernable difference between calcitriol and its analogues. Similarly, Colston et al., have shown that both calcitriol and calcipotriol reduce proliferation of MCF-7 breast cancer cells [54]. These findings point towards cancer-type specific sensitivities.

Based on the functional inhibition of the stem-like phenotype, we next performed gene expression analyses and confirmatory immunofluorescence staining showing that, aside from the strong and expected [15,55] increase of *CYP24A1*-expression, we observed

a highly significant and concentration-dependent reduction of the stemness markers *SOX2, OLIG2* with a concomitant increase in the differentiation marker *GFAP*. These findings indicate that calcitriol indeed reduces the stem-like phenotype of GSCs. This is further corroborated by the lack of changes in *CCND1*-expression, which indicates that the reduced sphere formation as shown using the LDAs is not due to inhibition of proliferation of calcitriol, but rather to prevention of sphere formation via blockage of the stem-like phenotype. We further reasoned that due to the reduction in stemness the GSCs might be more prone to conventional chemotherapy and we therefore wanted to put our hypothesis to test using an advanced, physiological *ex vivo* approach. Although, we only observed a very moderate trend in reduction of *BCL2* expression using qPCR, the *ex vivo* tumor growth assay of NCH644 GSCs showed that TMZ and calcitriol effectively synergize and can even result in the complete elimination of some tumors. Similarly, Bak et al. observed prolonged survival in TMZ and VitD$_3$-treated rats after orthotopic transplantation and attributed some of the combined effects to combined or rather enhanced activation of autophagy [24], with no changes in apoptosis-induction compared to TMZ-alone. A sensitization against conventional chemotherapeutics using VitD$_3$ or its analogs have also been observed in a variety of *in vivo* tumor models such as colorectal cancer [56] or prostate cancer [57]. Conversely, the *ex vivo* tumor growth assay with NCH421k GSCs showed stronger effects of TMZ alone and therefore no synergism with calcitriol. NCH644 cells are known to have an unmethylated MGMT-promoter with a high IC50 of TMZ in vitro (272 mM) [58] and thus are rather resistant to TMZ. In contrast, NCH421k have a methylated MGMT promoter and a lower IC50 of TMZ *in vitro* (200 μM) [58] and therefore are sensitive to TMZ. Thus, these experiments indicate that especially MGMT-expressing GSCs are particularly amenable towards calcitriol-based differentiation therapy, although a larger cohort of GSCs is necessary to foster this hypothesis.

Lastly, we performed a global proteomic analysis of NCH644 GSCs after treatment with calcitriol and could again confirm the reduction of the stemness marker proteins OLIG2 and SOX2, further validating our data and supporting the conclusion that calcitriol induces differentiation of GSCs. In addition, we could confirm that 5 of the 50 upregulated proteins are known VitD$_3$-targets according to Wikipathways (https://www.wikipathways.org/index.php/Pathway:WP2877, [59]). Surprisingly, an additional 5 upregulated proteins are related to Ca^{2+} signaling, indicating an involvement of Ca^{2+} in mediating the calcitriol-response. In fact, it is well-known that calcitriol can also induce non-genomic responses which involve the release of Ca^{2+} into the cytosol [13,15,60]. One of the upregulated Ca^{2+}-related proteins is RCAN1, whose expression is known to be induced via calmodulin-calcineurin-dependent Ca^{2+}-signaling [61,62] and VitD3 has been shown to also involve calmodulin-dependent signaling [63,64]. These data further indicate that at least a part of the calcitriol-effects is mediated via Ca^{2+}-signaling. Following this line-of-thought has been shown that Ca^{2+} is central to the maintenance of neural stem cells and often aberrantly regulated in GSCs [65]. Recently, the term calcium toolbox was proposed for the summary of all Ca^{2+}-related proteins in a cell and it was shown that GBM cells have a different composition of this toolbox compared to healthy brain tissue [66]. In a study by Leclerc et al. [67] the authors compared GSCs grown under stemness conditions to GSCs under serum growth for 7 and 30 days and termed this differentiated and senescent, respectively and applied to calcium toolbox by Robil et al., for a cluster analysis [66]. Interestingly, they found that 2 of the 5 Ca^{2+}-related proteins from our dataset (ANXA2 and S100A6) are associated with differentiated cells. These findings combined further corroborate our conclusion that calcitriol indeed induces differentiation and further provides a first mechanistic clue through changes in Ca^{2+}-signaling or binding proteins. This could also provide a mechanistic for the decreases effectiveness of the less-calcemic compound calcipotriol, which only induces genomic VitD$_3$-signaling, but not the non-genomic axis.

In summary we provide the first evidence that calcitriol can specifically reduce the stem-like phenotype of a subset of GSCs and potentially synergizes with TMZ in MGMT-expressing cells.

4. Materials and Methods

4.1. Cells and cell culture

For the experiments the following GSC lines were employed: 17/01 [29], 17/02 [29], GS-5 [28], GS-73 [36], the gliosarcoma line MNOF168 [35], MNOF1244 (see below), MNOF1300 [34], NCH421k [27], NCH481 [37] and NCH644 [27]. All cell lines except MNOF168, MNFO1244 and MNOF1300 were used and cultured in Neurobasal medium (Gibco, Darmstadt, Germany). The medium was supplemented with 1x B27, 100 U/ml Penicillin 100µg/mL Streptomycin (P/S, Gibco), 1 xGlutaMAX (Gibco), 20 ng/mL epidermal growth factor (EGF, Peprotech, Hamburg, Germany) 20 ng/ml and fibroblast growth factor (FGF, Peprotech). The GSCs MNOF168, MNOF1244 and MNOF1300 were grown in DMEM/F12 medium (Lonza, Basel, Switzerland) containing 20 ng/ml each of EGF and FGF, 20% BIT Admixture Supplement (Pelo Biotech, Planegg/Martinsried, Germany) and P/S. 17/01 is a primary cell line derived from a 51 year old female patient. [29]. 17/02 is a primary cell line obtained from a 60 year old patient after obtaining informed consent and ethics approval [29]. The tumor relapsed after percutaneous radiotherapy (60 Gy) and also chemotherapy with TMZ was performed. The cell line was prepared after a second, fractionated irradiation was done, followed by subtotal resection [29]. GS-5 and GS-73 were gifted by Katrin Lamszus (UKE Hamburg, Germany). MNOF168 and MNOF1300 are primary cultures provided by Stefan Momma and Julia Tichy (University Hospital Frankfurt, Germany) [34,35]. MNOF1244 is a primary cell culture obtained from a 69 year old female patient after obtaining informed consent and ethics approval (ethics committee at the University Hospital Frankfurt; reference number 04/09-SNO 01/11). Tumor tissue from the initial surgery prior to radiochemotherapy was dissociated and cultivated under serum-free culture conditions. Christel Herold-Mende (University Hospital Heidelberg, Germany) provided NCH421k, NCH481 and NCH644. HEK293T (ATCC #CRL-3216) were cultured in Dulbecco's modified Eagle's medium (DMEM GlutaMAX) supplied with heat-inactivated 10% FBS and 100 U/ml Penicillin 100 µg/ml Streptomycin (all from Gibco). GFP positive NCH644 and NCH421k were created by lentiviral transduction as described previously [68].

4.2. Compounds

$1,25(OH)_2D_3$ was purchased from Cayman Chemical. Using Ethanol (Sigma Aldrich) a stock solution was prepared and stored at - 20°C. Calcipotriol and TMZ were purchased from Sigma-Aldrich. Stock solutions have been dissolved with DMSO (Carl Roth GmbH) and stored at -20°C.

4.3. Limiting dilution assay

The limiting dilution assay was performed as described previously [29,30]. Briefly, 96 well plates were used to seed the cells in 200µl Neurobasal culture medium. By performing a row-wise descending dilution, cell concentrations of 8, 16, 32, 64, 128, 256, 512 and 1024 cells/well were reached for each cell line, while treatment was done with calcitriol/calcipotriol as indicated in the respective figures. The cells were treated immediately after treatment to ensure that single cells are treated and incubated for 7 days. Stem cell frequencies were assessed 7 days after seeding using extreme limiting dilution analysis (ELDA) software using the standard settings (http://bioinf.wehi.edu.au/software/elda; [31]). After microscopic evaluation the first two rows per plate were photographed using a Tecan Spark plate reader (Tecan, Grödig, Austria) and used for subsequent analyses. The Number and median size of spheres ≥250 µm were analyzed by FIJI [33] using a self-developed macro.

For NCH644 and 17/02 the wells after seeding 512 cells were employed and for GS-5 the wells after seeding 1024 cells were employed.

4.4. Tagman-based qRT-PCR

300.000 cells/well were seeded into 6-well plates and the following day treated with 50 nM calcitriol for 24h or 48 h. Experiments were performed using 3 biological replicates for each treatment condition, while the experiment was employed three times. RNA was isolated using the ExtractMe Total RNA Kit (Blirt S.A., Gdanks, Poland), while 1-2 µg RNA were used for cDNA synthesis. SuperScript III System (Life technologies, Darmstadt, Germany) allowed the synthesis of cDNA, whereas 100 U per sample was sufficient. The quantitative Real- Time PCR (qRT-PCR) was performed using Taqman probes (Applied Biosystems, Darmstadt, Geramany), Fast-Start Universal Probe Master Mix (Roche) on a StepOne Plus System (Applied Biosystems) in a 20 µl reaction volume. Ct values were normalized to TATA box binding protein (TBP). Fold change in gene expression was determined by $2^{-\Delta\Delta Ct}$ method, except for VDR-expression where the expression was determined using the $2^{-\Delta Ct}$ method.

The following Taqman-probes were used: BLC2 (Hs00608023_m1), CCND1 (Hs00765553_m1), CYP24A1 (Hs00167999_m1), GFAP (Hs00909233_m1), GLI1 (Hs00171790_m1), OLIG2 (Hs00300164_s1), SOX2 (Hs01053049_s1), SOX9 (Hs00165814_m1), TBP (Hs00427620_m1), TNC (Hs01115665_m1), VDR (Hs00172113_m1)

4.5. Immunofluorescence staining

8,000 cells/well were seeded in 8-well chambers and the following day treated for 24, 48, or 72h with 50 nM calcitriol or solvent. Slides were fixated using 4 % PFA before staining with the following primary antibodies: OLIG2 (R&D Systems, Minneapolis, Minnesota, USA), GFAP (Dako Cytomation, Glostrup, Denmark) SOX2 (R&D Systems, Minneapolis, Minnesota, USA) over night. Subsequently, slides were stained with a species-corresponding secondary antibody (goat anti-mouse (Alexa Fluor 594 F(ab')2 fragment IgG (H+L)); (goat anti-rabbit (Alexa Fluor 488 F(ab')2 fragment goat anti-rabbit IgG (H+L)); donkey anti-goat (Alexa Fluor 488 IgG (H+L))). Pictures were taken using a Nikon Eclipse TE2000-S fluorescent microscope operated by NIS elements software and adjusted using FIJI. Quantification was performed in Fiji by measuring the integrated density of the fluorescent signal (mean intensity of measured cell multiplied with the measured cell area) of 50 cells per condition using at least three pictures. The area was selected using the freehand selection tool, ensuring an exact and individual measurement for each cell. Violin Plots were generated using GraphPad Prism 9.

4.6. Proteomic Sample Preparation and data analyses

4.6.1. Sample preparation for LC-MS²

For protein extraction NCH644 GSCs were treated with 50 nM calcitriol one days after seeding. After 48h the cells were lysed in 2% SDS, 50 mM Tris-HCl pH8, 150 mM NaCl, 10 mM TCEP, 40 mM chloracetamide, protease inhibitor cocktail tablet (Sigma-Aldrich, Darmstadt, Germany) and "PhosStop" Phosphatase inhibitor tablet (Roche, Grenzach-Wyhlen, Germany) followed by sonication (1 ON/OFF, 30 s, 40%). Proteins were precipitated using methanol-chloroform extraction [69]. Proteins were digested with LysC (Wako Chemicals) and Trypsin (Promega, V5113) with the final ratio of 1:100 and digestion was performed overnight at 37°C and stopped by trifluoroaceticacid (TFA). The peptides purified using SepPak C18 columns (Waters, WAT054955). Eluates were dried and labeled with TMT reagents (ThermoFisher Scientific, 90061, TH266884) in 1:2 (w/w) ratio in 50 mM TEAB (SIGMA, 86600) with 20% acetonitrile. The reaction was quenched with hydroxylamine to a final concentration of 0.5% at RT and samples were pooled in equimolar ratio. At final, the peptides were fractionated using a High pH Reversed phase fractionation kit (ThermoFisher Scientific) according to manufacturer's instructions.

4.6.2. Mass spectrometry

Peptides were resuspended in 3% acetonitrile and 0.1% formic acid and separated on an Easy nLC 1200 (ThermoFisher Scientific) and a 22 cm long, 75 µm ID fused-silica column, which had been packed in house with 1.9 µm C18 particles (ReproSil-Pur, Dr. Maisch), and kept at 45°C using an integrated column oven (Sonation). Peptides were

eluted by a non-linear gradient from 5%–60% acetonitrile over 155 min and directly sprayed into a Orbitrap Fusion Lumos mass spectrometer equipped with a nanoFlex ion source (ThermoFisher Scientific) at a spray voltage of 2.3 kV [70][71]. For analysis 1/10 of each fraction was loaded onto the column. Each analysis used the Multi-Notch MS3-based TMT method [72] to reduce ion interference compared to MS2 quantification [73]. The scan sequence began with an MS1 spectrum (Orbitrap analysis; resolution 120,000 at 200 Th; mass range 350-1400 m/z; automatic gain control (AGC) target 400000; normalized AGC target 100%; maximum injection time 100 ms). Precursors for MS2 analysis were selected using 10 ms activation time method. MS2 analysis consisted of collision-induced dissociation (quadrupole ion trap analysis; Turbo scan rate; AGC 15000; normalized AGC target 150%; isolation window 0.7 Th; normalized collision energy (NCE) 35; maximum injection time 50 ms). Monoisotopic peak assignment was used and previously interrogated precursors were excluded using a dynamic window (150 s ± 7 ppm) and dependent scans were per- formed on a single charge state per precursor. Following acquisition of each MS2 spectrum, a synchronous-precursor-selection (SPS) MS3 scan was collected on the top 10 most intense ions in the MS2 spectrum [72]. MS3 precursors were fragmented by high energy collision-induced dissociation (HCD) and analyzed using the Orbitrap (NCE 65; AGC 100000; normalized AGC target 200%; maximum injection time 150 ms, resolution was 15,000 at 200 Th).

4.6.3. Data analysis

Raw data were analyzed with Proteome Discoverer (PD) 2.4 (ThermoFisher Scientific) and SequenceHT node was selected for database searches. Human trypsin digested proteome (Homo sapiens SwissProt database [TaxID:9606, version 2020-03-12]) was used for protein identifications. Contaminants (MaxQuant "contamination.fasta") were determined for quality control. TMT6 (+229.163) at the N-terminus, TMT6 (K, +229.163) at lysine and carbamidomethyl (+57.021) at cysteine residues were set as fixed modifications. Methionine oxidation (M, +15.995) and acetylation (+42.011) at the protein N-terminus were set for dynamic modifications. Precursor mass tolerance was set to 7 ppm and fragment mass tolerance was set to 0.5 Da. Default Percolator settings in PD were used to filter perfect spectrum matches (PSMs). Reporter ion quantification was achieved with default settings in consensus workflow. Protein file from PD was then exported to Excel for further processing. Normalized abundances from protein file were used for statistical analysis after contaminations and complete empty values removed. Significantly altered proteins were determined by a two-sided, unpaired Student`s t-test (p-value < 0.05) adding minimum fold-change cut-off (> = 0.5) with R version 4.0.2 [74] in RStudio [75]. Gplots version 3.1.1 [76] was used to visualize heatmaps and EnhancedVolcano version 1.6.0 [77] was used for volcano plot. Figures later then edited with Adobe Illustrator CS5. The mass spectrometry proteomics data have been deposited to the ProteomeXchange Consortium via the PRIDE [78] partner repository with the dataset identifier PXD026789 (Username: reviewer_pxd026789@ebi.ac.uk; Password: ytAmnUJy).

4.7. Lentiviral transduction of GSCs

GFP-positive NCH644 cells were created by using pLV[Exp]-EGFP/Puro-CMV>Stuffer300 (Vectorbuilder GmbH, Neu-Isenburg, Germany) . 150,000 HEK293T cells were seeded in 6 well plates and were allowed to incubate overnight. For transfection 2 μg plasmid DNA (pLKO.1-puro), 1.5 μg gag/pol plasmid (psPAX2, addgene #12260) and 0.5 μg VSV-G envelope plasmid (pMD2.G, addgene #12259) were used in 57 μl Opti-MEM and 6 μl FuGENE HD (Promega, Fitchburg, WI, USA) transfection reagent. 6 hours later the medium was changed, while the viral supernatant was collected and later pooled, as well as filtered through a 0.45 μm filter. The viral supernatant was diluted 1:1 with medium and 8 μg/ml protamine sulfate in PBS was added (Sigma-Aldrich). 30,000 freshly dissociated cells were incubated for at least 48h in virus-containing medium. Selection of positively transduced cells was ensured by adding 2 μg/ml or 1 μg/ml Puromycin to cul-

ture medium for NCH644 and NCH421k, respectively. Transduction efficiency was determined by FACS measurement and was 91, 6% for NCH644 GFP positive cells (NCH644 GFP+) and 81.91% for GFP-positive NCH421k cells (NCH421k GFP+). psPAX2 was a gift from Didier Trono (Addgene plasmid # 12260 ; http://n2t.net/addgene:12260 ; RRID:Addgene_12260). pMD2.G was a gift from Didier Trono (Addgene plasmid # 12259 ; http://n2t.net/addgene:12259 ; RRID:Addgene_12259)

487. Adult Organotypic Slice Cultures and Ex Vivo Tumor Growth assay

Adult organotypic slice culture (OTC) was carried out based on the method described previously [29,41]. Mouse brains were dissected and dura mater was removed. Subsequently, mouse brains were placed in warm (35-40 °C) 2% low-melting agarose (Carl Roth). A Vibratome VT1000 (Leica, Wetzlar, Germany) was used to create evenly sized 150 µm transverse sections. The sections were placed on Millicell cell culture inserts (Merck KGaA, Darmstadt, Germany) and cultured in 6- well plates using FCS-free medium consisting of DMEM/F12 supplied with 1x B27 and 1x N2 supplement and 100 U/ml Penicillin 100 µg/ml Streptomycin(all from Gibco). One day later, multiple spheres were placed on the mouse brain slices. Adequate spheres were prepared by seeding 3 000 NCH644 GFP positive cells/well in u- shaped 96- well plates using 200µl Medium. Spheres were allowed to grow for 3 days. One day after sphere transplantion pictures were taken (day 0) and the treatment was started, which was refreshed 3 times per week. Tumor growth was evaluated using FIJI, after pictures have been taken regularly by Nikon SMZ25 stereomicroscope equipped with a P2-SHR Plan Apo 2 x objective operated by NIS elements software. As the tumor size was normalized to the size on day 0, growth curves were created.

4.9. Statistics

Statistical analyses involved One-way and Two-way ANOVA using GraphPad Prism 7 (GraphPad Prism 7 (GraphPad Software, La Jolla, CA, USA) with the respective Post-Hoc-test as indicated. For LDA the statistical evaluation was taken from ELDA software, which calculates statistical significance based on a Chi^2-Square-Test [31].

5. Conclusions

Here, we show that therapeutic doses of the hormonally active form of VitD$_3$, calcitriol, carry potential as an anti-glioblastoma therapy. We demonstrate that calcitriol reduces the sphere-forming potential of GSCs *in vitro*, which was accompanied by reduced stemness marker gene expression and increased differentiation marker expression. Most importantly, using adult OTCs as a physiological and complex model system, we show that calcitriol not only hinders tumor growth as a single agent, but also potently synergizes with the current standard-of-care TMZ. These promising findings emphasize that future research should be focusing on further delineating the effects of calcitriol, a safe and well-known drug, and its application as an adjuvant therapy for GBM.

Author Contributions:

Conceptualization, Benedikt Linder; Data curation, Süleyman Bozkurt, Marina Hoffmann and Benedikt Linder; Formal analysis, Julia Gerstmeier, Anna-Lena Possmayer, Süleyman Bozkurt, Marina Hoffmann, Christian Münch and Benedikt Linder; Investigation, Julia Gerstmeier, Anna-Lena Possmayer, Süleyman Bozkurt, Marina Hoffmann and Benedikt Linder; Methodology, Julia Gerstmeier, Süleyman Bozkurt, Marina Hoffmann and Benedikt Linder; Project administration, Benedikt Linder; Resources, Ivan Dikic, Christel Herold-Mende, Michael Burger, Christian Münch and Donat Kögel; Software, Süleyman Bozkurt, Marina Hoffmann, Christian Münch and Benedikt Linder; Supervision, Donat Kögel and Benedikt Linder; Validation, Benedikt Linder; Visualization, Julia Gerstmeier, Anna-Lena Possmayer, Süleyman Bozkurt and Benedikt Linder; Writing – original draft, Julia Gerstmeier, Anna-Lena Possmayer, Süleyman Bozkurt, Marina Hoffmann, Michael Burger, Donat Kögel and Benedikt Linder; Writing – review & editing, Donat Kögel and Benedikt Linder.

References

1. Louis, D.N.; Perry, A.; Reifenberger, G.; von Deimling, A.; Figarella-Branger, D.; Cavenee, W.K.; Ohgaki, H.; Wiestler, O.D.; Kleihues, P.; Ellison, D.W. The 2016 World Health Organization Classification of Tumors of the Central Nervous System: a summary. *Acta Neuropathol* **2016**, *131*, 803-820, doi:10.1007/s00401-016-1545-1.

2. Berger, T.R.; Wong, E.T. Tumor treating fields in neuro-oncology: integration of alternating electric fields therapy into promising treatment strategies. *Chin Clin Oncol* **2020**, 10.21037/cco.2020.02.04, doi:10.21037/cco.2020.02.04.

3. Mittal, S.; Klinger, N.V.; Michelhaugh, S.K.; Barger, G.R.; Pannullo, S.C.; Juhasz, C. Alternating electric tumor treating fields for treatment of glioblastoma: rationale, preclinical, and clinical studies. *J Neurosurg* **2018**, *128*, 414-421, doi:10.3171/2016.9.JNS16452.

4. Giladi, M.; Weinberg, U.; Schneiderman, R.S.; Porat, Y.; Munster, M.; Voloshin, T.; Blatt, R.; Cahal, S.; Itzhaki, A.; Onn, A., et al. Alternating electric fields (tumor-treating fields therapy) can improve chemotherapy treatment efficacy in non-small cell lung cancer both in vitro and in vivo. *Semin Oncol* **2014**, *41 Suppl 6*, S35-41, doi:10.1053/j.seminoncol.2014.09.006.

5. Rominiyi, O.; Vanderlinden, A.; Clenton, S.J.; Bridgewater, C.; Al-Tamimi, Y.; Collis, S.J. Tumour treating fields therapy for glioblastoma: current advances and future directions. *Br J Cancer* **2021**, *124*, 697-709, doi:10.1038/s41416-020-01136-5.

6. Butler, M.; Pongor, L.; Su, Y.T.; Xi, L.; Raffeld, M.; Quezado, M.; Trepel, J.; Aldape, K.; Pommier, Y.; Wu, J. MGMT Status as a Clinical Biomarker in Glioblastoma. *Trends Cancer* **2020**, *6*, 380-391, doi:10.1016/j.trecan.2020.02.010.

7. Luwor, R.B.; Baradaran, B.; Taylor, L.E.; Iaria, J.; Nheu, T.V.; Amiry, N.; Hovens, C.M.; Wang, B.; Kaye, A.H.; Zhu, H.J. Targeting Stat3 and Smad7 to restore TGF-beta cytostatic regulation of tumor cells in vitro and in vivo. *Oncogene* **2013**, *32*, 2433-2441, doi:10.1038/onc.2012.260.

8. Bradshaw, A.; Wickremsekera, A.; Tan, S.T.; Peng, L.; Davis, P.F.; Itinteang, T. Cancer Stem Cell Hierarchy in Glioblastoma Multiforme. *Front Surg* **2016**, *3*, 21, doi:10.3389/fsurg.2016.00021.

9. Soeda, A.; Park, M.; Lee, D.; Mintz, A.; Androutsellis-Theotokis, A.; McKay, R.D.; Engh, J.; Iwama, T.; Kunisada, T.; Kassam, A.B., et al. Hypoxia promotes expansion of the CD133-positive glioma stem cells through activation of HIF-1alpha. *Oncogene* **2009**, *28*, 3949-3959, doi:10.1038/onc.2009.252.

10. Gilbertson, R.J.; Rich, J.N. Making a tumour's bed: glioblastoma stem cells and the vascular niche. *Nat Rev Cancer* **2007**, *7*, 733-736, doi:10.1038/nrc2246.

11. Hide, T.; Shibahara, I.; Kumabe, T. Novel concept of the border niche: glioblastoma cells use oligodendrocytes progenitor cells (GAOs) and microglia to acquire stem cell-like features. *Brain Tumor Pathol* **2019**, *36*, 63-73, doi:10.1007/s10014-019-00341-2.

12. DeLuca, H.F. Overview of general physiologic features and functions of vitamin D. *Am J Clin Nutr* **2004**, *80*, 1689S-1696S, doi:10.1093/ajcn/80.6.1689S.

13.   Negri, M.; Gentile, A.; de Angelis, C.; Monto, T.; Patalano, R.; Colao, A.; Pivonello, R.; Pivonello, C. Vitamin D-Induced Molecular Mechanisms to Potentiate Cancer Therapy and to Reverse Drug-Resistance in Cancer Cells. *Nutrients* **2020**, *12*, doi:10.3390/nu12061798.

14.   Christakos, S.; Ajibade, D.V.; Dhawan, P.; Fechner, A.J.; Mady, L.J. Vitamin D: metabolism. *Endocrinol Metab Clin North Am* **2010**, *39*, 243-253, table of contents, doi:10.1016/j.ecl.2010.02.002.

15.   Deeb, K.K.; Trump, D.L.; Johnson, C.S. Vitamin D signalling pathways in cancer: potential for anticancer therapeutics. *Nat Rev Cancer* **2007**, *7*, 684-700, doi:10.1038/nrc2196.

16.   Bikle, D.D. The vitamin D receptor: a tumor suppressor in skin. *Discov Med* **2011**, *11*, 7-17.

17.   Hu, P.; Li, S.; Tian, N.; Wu, F.; Hu, Y.; Li, D.; Qi, Y.; Wei, Z.; Wei, Q.; Li, Y., et al. Acidosis enhances the self-renewal and mitochondrial respiration of stem cell-like glioma cells through CYP24A1-mediated reduction of vitamin D. *Cell Death Dis* **2019**, *10*, 25, doi:10.1038/s41419-018-1242-1.

18.   Takahashi, H.; Cornish, A.J.; Sud, A.; Law, P.J.; Kinnersley, B.; Ostrom, Q.T.; Labreche, K.; Eckel-Passow, J.E.; Armstrong, G.N.; Claus, E.B., et al. Mendelian randomisation study of the relationship between vitamin D and risk of glioma. *Sci Rep* **2018**, *8*, 2339, doi:10.1038/s41598-018-20844-w.

19.   Zigmont, V.; Garrett, A.; Peng, J.; Seweryn, M.; Rempala, G.A.; Harris, R.; Holloman, C.; Gundersen, T.E.; Ahlbom, A.; Feychting, M., et al. Association Between Prediagnostic Serum 25-Hydroxyvitamin D Concentration and Glioma. *Nutr Cancer* **2015**, *67*, 1120-1130, doi:10.1080/01635581.2015.1073757.

20.   Salomon, D.G.; Fermento, M.E.; Gandini, N.A.; Ferronato, M.J.; Arevalo, J.; Blasco, J.; Andres, N.C.; Zenklusen, J.C.; Curino, A.C.; Facchinetti, M.M. Vitamin D receptor expression is associated with improved overall survival in human glioblastoma multiforme. *J Neurooncol* **2014**, *118*, 49-60, doi:10.1007/s11060-014-1416-3.

21.   Norlin, M. Effects of vitamin D in the nervous system: Special focus on interaction with steroid hormone signalling and a possible role in the treatment of brain cancer. *J Neuroendocrinol* **2020**, *32*, e12799, doi:10.1111/jne.12799.

22.   Elmaci, I.; Ozpinar, A.; Ozpinar, A.; Perez, J.L.; Altinoz, M.A. From epidemiology and neurometabolism to treatment: Vitamin D in pathogenesis of glioblastoma Multiforme (GBM) and a proposal for Vitamin D + all-trans retinoic acid + Temozolomide combination in treatment of GBM. *Metab Brain Dis* **2019**, *34*, 687-704, doi:10.1007/s11011-019-00412-5.

23.   Maleklou, N.; Allameh, A.; Kazemi, B. Preparation, characterization and in vitro-targeted delivery of novel Apolipoprotein E-based nanoparticles to C6 glioma with controlled size and loading efficiency. *J Drug Target* **2016**, *24*, 348-358, doi:10.3109/1061186X.2015.1077849.

24.   Bak, D.H.; Kang, S.H.; Choi, D.R.; Gil, M.N.; Yu, K.S.; Jeong, J.H.; Lee, N.S.; Lee, J.H.; Jeong, Y.G.; Kim, D.K., et al. Autophagy enhancement contributes to the synergistic effect of vitamin D in temozolomide-based glioblastoma chemotherapy. *Exp Ther Med* **2016**, *11*, 2153-2162, doi:10.3892/etm.2016.3196.

25.   Sui, A.; Xu, Y.; Pan, B.; Guo, T.; Wu, J.; Shen, Y.; Yang, J.; Guo, X. Histone demethylase KDM6B regulates 1,25-dihydroxyvitamin D3-induced senescence in glioma cells. *J Cell Physiol* **2019**, *234*, 17990-17998, doi:10.1002/jcp.28431.

26.   Trouillas, P.; Honnorat, J.; Bret, P.; Jouvet, A.; Gerard, J.P. Redifferentiation therapy in brain tumors: long-lasting complete regression of glioblastomas and an anaplastic astrocytoma under long term 1-alpha-hydroxycholecalciferol. *J Neurooncol* **2001**, *51*, 57-66, doi:10.1023/a:1006437003352.

27.   Campos, B.; Wan, F.; Farhadi, M.; Ernst, A.; Zeppernick, F.; Tagscherer, K.E.; Ahmadi, R.; Lohr, J.; Dictus, C.; Gdynia, G., et al. Differentiation therapy exerts antitumor effects on stem-like glioma cells. *Clin Cancer Res* **2010**, *16*, 2715-2728, doi:10.1158/1078-0432.CCR-09-1800.

28.   Gunther, H.S.; Schmidt, N.O.; Phillips, H.S.; Kemming, D.; Kharbanda, S.; Soriano, R.; Modrusan, Z.; Meissner, H.; Westphal, M.; Lamszus, K. Glioblastoma-derived stem cell-enriched cultures form distinct subgroups according to molecular and phenotypic criteria. *Oncogene* **2008**, *27*, 2897-2909, doi:10.1038/sj.onc.1210949.

29.   Linder, B.; Wehle, A.; Hehlgans, S.; Bonn, F.; Dikic, I.; Rodel, F.; Seifert, V.; Kogel, D. Arsenic Trioxide and (-)-Gossypol Synergistically Target Glioma Stem-Like Cells via Inhibition of Hedgehog and Notch Signaling. *Cancers (Basel)* **2019**, *11*, doi:10.3390/cancers11030350.

30.   Rahman, M.; Reyner, K.; Deleyrolle, L.; Millette, S.; Azari, H.; Day, B.W.; Stringer, B.W.; Boyd, A.W.; Johns, T.G.; Blot, V., et al. Neurosphere and adherent culture conditions are equivalent for malignant glioma stem cell lines. *Anat Cell Biol* **2015**, *48*, 25-35, doi:10.5115/acb.2015.48.1.25.

31.   Hu, Y.; Smyth, G.K. ELDA: extreme limiting dilution analysis for comparing depleted and enriched populations in stem cell and other assays. *J Immunol Methods* **2009**, *347*, 70-78, doi:10.1016/j.jim.2009.06.008.

32.   Nagpal, S.; Na, S.; Rathnachalam, R. Noncalcemic actions of vitamin D receptor ligands. *Endocr Rev* **2005**, *26*, 662-687, doi:10.1210/er.2004-0002.

33.   Schindelin, J.; Arganda-Carreras, I.; Frise, E.; Kaynig, V.; Longair, M.; Pietzsch, T.; Preibisch, S.; Rueden, C.; Saalfeld, S.; Schmid, B., et al. Fiji: an open-source platform for biological-image analysis. *Nat Methods* **2012**, *9*, 676-682, doi:10.1038/nmeth.2019.

34.   Genssler, S.; Burger, M.C.; Zhang, C.; Oelsner, S.; Mildenberger, I.; Wagner, M.; Steinbach, J.P.; Wels, W.S. Dual targeting of glioblastoma with chimeric antigen receptor-engineered natural killer cells overcomes heterogeneity of target antigen expression and enhances antitumor activity and survival. *Oncoimmunology* **2016**, *5*, e1119354, doi:10.1080/2162402X.2015.1119354.

35.   Zhang, C.; Burger, M.C.; Jennewein, L.; Genssler, S.; Schonfeld, K.; Zeiner, P.; Hattingen, E.; Harter, P.N.; Mittelbronn, M.; Tonn, T., et al. ErbB2/HER2-Specific NK Cells for Targeted Therapy of Glioblastoma. *J Natl Cancer Inst* **2016**, *108*, doi:10.1093/jnci/djv375.

36.   Maire, C.L.; Fuh, M.M.; Kaulich, K.; Fita, K.D.; Stevic, I.; Heiland, D.H.; Welsh, J.A.; Jones, J.C.; Gorgens, A.; Ricklefs, T., et al. Genome-wide methylation profiling of glioblastoma cell-derived extracellular vesicle DNA allows tumor classification. *Neuro Oncol* **2021**, 10.1093/neuonc/noab012, doi:10.1093/neuonc/noab012.

37.   Gobin, M.; Nazarov, P.V.; Warta, R.; Timmer, M.; Reifenberger, G.; Felsberg, J.; Vallar, L.; Chalmers, A.J.; Herold-Mende, C.C.; Goldbrunner, R., et al. A DNA Repair and Cell-Cycle Gene Expression Signature in Primary and Recurrent Glioblastoma: Prognostic Value and Clinical Implications. *Cancer Res* **2019**, *79*, 1226-1238, doi:10.1158/0008-5472.CAN-18-2076.

38.   Clement, V.; Sanchez, P.; de Tribolet, N.; Radovanovic, I.; Ruiz i Altaba, A. HEDGEHOG-GLI1 signaling regulates human glioma growth, cancer stem cell self-renewal, and tumorigenicity. *Curr Biol* **2007**, *17*, 165-172, doi:10.1016/j.cub.2006.11.033.

39.   Bijlsma, M.F.; Spek, C.A.; Zivkovic, D.; van de Water, S.; Rezaee, F.; Peppelenbosch, M.P. Repression of smoothened by patched-dependent (pro-)vitamin D3 secretion. *PLoS Biol* **2006**, *4*, e232, doi:10.1371/journal.pbio.0040232.

40.   Linder, B.; Weber, S.; Dittmann, K.; Adamski, J.; Hahn, H.; Uhmann, A. A Functional and Putative Physiological Role of Calcitriol in Patched1/Smoothened Interaction. *J Biol Chem* **2015**, *290*, 19614-19628, doi:10.1074/jbc.M115.646141.

41.   Remy, J.; Linder, B.; Weirauch, U.; Konovalova, J.; Marschalek, R.; Aigner, A.; Kogel, D. Inhibition of PIM1 blocks the autophagic flux to sensitize glioblastoma cells to ABT-737-induced apoptosis. *Biochim Biophys Acta Mol Cell Res* **2018**, 10.1016/j.bbamcr.2018.10.017, doi:10.1016/j.bbamcr.2018.10.017.

42. Lan, X.; Jorg, D.J.; Cavalli, F.M.G.; Richards, L.M.; Nguyen, L.V.; Vanner, R.J.; Guilhamon, P.; Lee, L.; Kushida, M.M.; Pellacani, D., et al. Fate mapping of human glioblastoma reveals an invariant stem cell hierarchy. *Nature* **2017**, *549*, 227-232, doi:10.1038/nature23666.

43. D'Arcy, M.S. Cell death: a review of the major forms of apoptosis, necrosis and autophagy. *Cell Biol Int* **2019**, *43*, 582-592, doi:10.1002/cbin.11137.

44. Filatova, A.; Acker, T.; Garvalov, B.K. The cancer stem cell niche(s): the crosstalk between glioma stem cells and their microenvironment. *Biochim Biophys Acta* **2013**, *1830*, 2496-2508, doi:10.1016/j.bbagen.2012.10.008.

45. Ahmed, A.U.; Auffinger, B.; Lesniak, M.S. Understanding glioma stem cells: rationale, clinical relevance and therapeutic strategies. *Expert Rev Neurother* **2013**, *13*, 545-555, doi:10.1586/ern.13.42.

46. Gilbert, C.A.; Ross, A.H. Cancer stem cells: cell culture, markers, and targets for new therapies. *J Cell Biochem* **2009**, *108*, 1031-1038, doi:10.1002/jcb.22350.

47. Beier, D.; Hau, P.; Proescholdt, M.; Lohmeier, A.; Wischhusen, J.; Oefner, P.J.; Aigner, L.; Brawanski, A.; Bogdahn, U.; Beier, C.P. CD133(+) and CD133(-) glioblastoma-derived cancer stem cells show differential growth characteristics and molecular profiles. *Cancer Res* **2007**, *67*, 4010-4015, doi:10.1158/0008-5472.CAN-06-4180.

48. Bao, S.; Wu, Q.; McLendon, R.E.; Hao, Y.; Shi, Q.; Hjelmeland, A.B.; Dewhirst, M.W.; Bigner, D.D.; Rich, J.N. Glioma stem cells promote radioresistance by preferential activation of the DNA damage response. *Nature* **2006**, *444*, 756-760, doi:10.1038/nature05236.

49. Bikle, D.D.; Elalieh, H.; Welsh, J.; Oh, D.; Cleaver, J.; Teichert, A. Protective role of vitamin D signaling in skin cancer formation. *J Steroid Biochem Mol Biol* **2013**, *136*, 271-279, doi:10.1016/j.jsbmb.2012.09.021.

50. Emanuelsson, I.; Wikvall, K.; Friman, T.; Norlin, M. Vitamin D Analogues Tacalcitol and Calcipotriol Inhibit Proliferation and Migration of T98G Human Glioblastoma Cells. *Basic Clin Pharmacol Toxicol* **2018**, *123*, 130-136, doi:10.1111/bcpt.13007.

51. Arensman, M.D.; Nguyen, P.; Kershaw, K.M.; Lay, A.R.; Ostertag-Hill, C.A.; Sherman, M.H.; Downes, M.; Liddle, C.; Evans, R.M.; Dawson, D.W. Calcipotriol Targets LRP6 to Inhibit Wnt Signaling in Pancreatic Cancer. *Mol Cancer Res* **2015**, *13*, 1509-1519, doi:10.1158/1541-7786.MCR-15-0204.

52. Gorchs, L.; Ahmed, S.; Mayer, C.; Knauf, A.; Fernandez Moro, C.; Svensson, M.; Heuchel, R.; Rangelova, E.; Bergman, P.; Kaipe, H. The vitamin D analogue calcipotriol promotes an anti-tumorigenic phenotype of human pancreatic CAFs but reduces T cell mediated immunity. *Sci Rep* **2020**, *10,* 17444, doi:10.1038/s41598-020-74368-3.

53. Segovia-Mendoza, M.; Diaz, L.; Gonzalez-Gonzalez, M.E.; Martinez-Reza, I.; Garcia-Quiroz, J.; Prado-Garcia, H.; Ibarra-Sanchez, M.J.; Esparza-Lopez, J.; Larrea, F.; Garcia-Becerra, R. Calcitriol and its analogues enhance the antiproliferative activity of gefitinib in breast cancer cells. *J Steroid Biochem Mol Biol* **2015**, *148*, 122-131, doi:10.1016/j.jsbmb.2014.12.006.

54. Colston, K.W.; Chander, S.K.; Mackay, A.G.; Coombes, R.C. Effects of synthetic vitamin D analogues on breast cancer cell proliferation in vivo and in vitro. *Biochem Pharmacol* **1992**, *44*, 693-702, doi:10.1016/0006-2952(92)90405-8.

55. Haussler, M.R.; Whitfield, G.K.; Haussler, C.A.; Hsieh, J.C.; Thompson, P.D.; Selznick, S.H.; Dominguez, C.E.; Jurutka, P.W. The nuclear vitamin D receptor: biological and molecular regulatory properties revealed. *J Bone Miner Res* **1998**, *13*, 325-349, doi:10.1359/jbmr.1998.13.3.325.

56. Li, W.; Wang, Q.L.; Liu, X.; Dong, S.H.; Li, H.X.; Li, C.Y.; Guo, L.S.; Gao, J.M.; Berger, N.A.; Li, L., et al. Combined use of vitamin D3 and metformin exhibits synergistic chemopreventive effects on colorectal neoplasia in rats and mice. *Cancer Prev Res (Phila)* **2015**, *8*, 139-148, doi:10.1158/1940-6207.CAPR-14-0128.

57.   Santucci, K.L.; Snyder, K.K.; Baust, J.M.; Van Buskirk, R.G.; Mouraviev, V.; Polascik, T.J.; Gage, A.A.; Baust, J.G. Use of 1,25alpha dihydroxyvitamin D3 as a cryosensitizing agent in a murine prostate cancer model. *Prostate Cancer Prostatic Dis* **2011**, *14*, 97-104, doi:10.1038/pcan.2010.52.

58.   Dirkse, A.; Golebiewska, A.; Buder, T.; Nazarov, P.V.; Muller, A.; Poovathingal, S.; Brons, N.H.C.; Leite, S.; Sauvageot, N.; Sarkisjan, D., et al. Stem cell-associated heterogeneity in Glioblastoma results from intrinsic tumor plasticity shaped by the microenvironment. *Nat Commun* **2019**, *10*, 1787, doi:10.1038/s41467-019-09853-z.

59.   Fijten, R.d.N., Kim; Kutmon, Martina; Pico, Alexander; Ehrhart, Friederike; Hanspers, Krisitna; Willighagen, Egon; Weitz, Eric. Vitamin D receptor pathway. Availabe online: https://www.wikipathways.org/index.php/Pathway:WP2877 (accessed on 27.05.2021).

60.   Khammissa, R.A.G.; Fourie, J.; Motswaledi, M.H.; Ballyram, R.; Lemmer, J.; Feller, L. The Biological Activities of Vitamin D and Its Receptor in Relation to Calcium and Bone Homeostasis, Cancer, Immune and Cardiovascular Systems, Skin Biology, and Oral Health. *Biomed Res Int* **2018**, *2018*, 9276380, doi:10.1155/2018/9276380.

61.   Hirakawa, Y.; Nary, L.J.; Medh, R.D. Glucocorticoid evoked upregulation of RCAN1-1 in human leukemic CEM cells susceptible to apoptosis. *J Mol Signal* **2009**, *4*, 6, doi:10.1186/1750-2187-4-6.

62.   Torac, E.; Gaman, L.; Atanasiu, V. The regulator of calcineurin (RCAN1) an important factor involved in atherosclerosis and cardiovascular diseases development. *J Med Life* **2014**, *7*, 481-487.

63.   Bikle, D.D.; Munson, S. 1,25-Dihydroxyvitamin D increases calmodulin binding to specific proteins in the chick duodenal brush border membrane. *J Clin Invest* **1985**, *76*, 2312-2316, doi:10.1172/JCI112241.

64.   Nimitphong, H.; Park, E.; Lee, M.J. Vitamin D regulation of adipogenesis and adipose tissue functions. *Nutr Res Pract* **2020**, *14*, 553-567, doi:10.4162/nrp.2020.14.6.553.

65.   Coronas, V.; Terrie, E.; Deliot, N.; Arnault, P.; Constantin, B. Calcium Channels in Adult Brain Neural Stem Cells and in Glioblastoma Stem Cells. *Front Cell Neurosci* **2020**, *14*, 600018, doi:10.3389/fncel.2020.600018.

66.   Robil, N.; Petel, F.; Kilhoffer, M.C.; Haiech, J. Glioblastoma and calcium signaling--analysis of calcium toolbox expression. *Int J Dev Biol* **2015**, *59*, 407-415, doi:10.1387/ijdb.150200jh.

67.   Leclerc, C.; Haeich, J.; Aulestia, F.J.; Kilhoffer, M.C.; Miller, A.L.; Neant, I.; Webb, S.E.; Schaeffer, E.; Junier, M.P.; Chneiweiss, H., et al. Calcium signaling orchestrates glioblastoma development: Facts and conjunctures. *Biochim Biophys Acta* **2016**, *1863*, 1447-1459, doi:10.1016/j.bbamcr.2016.01.018.

68.   Meyer, N.; Henkel, L.; Linder, B.; Zielke, S.; Tascher, G.; Trautmann, S.; Geisslinger, G.; Münch, C.; Fulda, S.; Tegeder, I., et al. Autophagy activation, lipotoxicity and lysosomal membrane permeabilization synergize to promote pimozide- and loperamide-induced glioma cell death. *bioRxiv* **2020**, 10.1101/2020.09.23.309617, doi:10.1101/2020.09.23.309617.

69.   Sapcariu, S.C.; Kanashova, T.; Weindl, D.; Ghelfi, J.; Dittmar, G.; Hiller, K. Simultaneous extraction of proteins and metabolites from cells in culture. *MethodsX* **2014**, *1*, 74-80, doi:10.1016/j.mex.2014.07.002.

70.   Hosp, F.; Scheltema, R.A.; Eberl, H.C.; Kulak, N.A.; Keilhauer, E.C.; Mayr, K.; Mann, M. A Double-Barrel Liquid Chromatography-Tandem Mass Spectrometry (LC-MS/MS) System to Quantify 96 Interactomes per Day. *Mol Cell Proteomics* **2015**, *14*, 2030-2041, doi:10.1074/mcp.O115.049460.

71.   Kelstrup, C.D.; Young, C.; Lavallee, R.; Nielsen, M.L.; Olsen, J.V. Optimized fast and sensitive acquisition methods for shotgun proteomics on a quadrupole orbitrap mass spectrometer. *J Proteome Res* **2012**, *11*, 3487-3497, doi:10.1021/pr3000249.

72.   McAlister, G.C.; Nusinow, D.P.; Jedrychowski, M.P.; Wuhr, M.; Huttlin, E.L.; Erickson, B.K.; Rad, R.; Haas, W.; Gygi, S.P. MultiNotch MS3 enables accurate, sensitive, and multiplexed detection of differential expression across cancer cell line proteomes. *Anal Chem* **2014**, *86*, 7150-7158, doi:10.1021/ac502040v.

73. Paulo, J.A.; O'Connell, J.D.; Gygi, S.P. A Triple Knockout (TKO) Proteomics Standard for Diagnosing Ion Interference in Isobaric Labeling Experiments. *J Am Soc Mass Spectrom* **2016**, *27*, 1620-1625, doi:10.1007/s13361-016-1434-9.

74. R Core Team *R: A Language and Environment for Statistical Computing*, 4.0.2.; R Foundation for Statistical Computing: Vienna, Austria, 2020.

75. RStudio Team *RStudio: Integrated Development for R. RStudio*, PBC, Boston, MA, 2020.

76. Warnes, G.R.B., Ben; Bonebakker, Lodewijk; Gentleman, Robert; Huber, Wolfgang; Liaw, Andy; Lumley, Thomas; Maechler, Martin; Magnusson, Arni; Moeller, Steffen; Schwartz, Marc, Venables, Bill *gplots: Various R programming tools for plotting data*, 2020.

77. Blighe, K.R., Sharmila; Lewis, Myles *EnhancedVolcano: Publication-ready volcano plots with enhanced colouring and labeling*, R package version 1.6.0. ; 2020.

78. Perez-Riverol, Y.; Csordas, A.; Bai, J.; Bernal-Llinares, M.; Hewapathirana, S.; Kundu, D.J.; Inuganti, A.; Griss, J.; Mayer, G.; Eisenacher, M., et al. The PRIDE database and related tools and resources in 2019: improving support for quantification data. *Nucleic Acids Res* **2019**, *47*, D442-D450, doi:10.1093/nar/gky1106.